

AN ABSTRACT OF THE THESIS OF

Ajeet K Johnson for the degree of Master of Science in Geology presented on January 18, 2011

Title: Dextral shear and north-directed crustal shortening defines the transition between extensional and contractional provinces in north-central Oregon

Abstract approved:

Andrew J. Meigs

Distributed deformation in the backarc of Cascadia is complex. Off the west coast lies the Cascadia convergent margin. East of the plate boundary, clockwise rotation of the Oregon Coast Range block with respect to stable North America influences backarc deformation, causing extensional faults in southeast Oregon, contraction folding in southeast Washington and a transition between the two opposing styles in north-central Oregon. Folding of the Mutton Mountain and Tygh Ridge anticlines commenced post 15.5 Ma and was most active between ~8.4 and 2.6 Ma. From Mutton Mountain to Tygh Ridge anticlines, minimum estimates of north-south shortening give an average shortening rate of 0.14 mm/yr from 8.4 to 2.6 Ma. Change in strike and dextral offsets of axial traces reflects a broad shear zone transferring motion between two relatively stable blocks; the Ochoco Mountain block and the Cascade arc. The transition region is characterized where dextral shear accommodates for an west-east velocity gradient. GPS velocity vectors indicate a difference of 1.0 mm/yr from the northern Basin and Range to the north and ~0.8 mm/yr from west to east.

© Copyright by Ajeet K Johnson

January 18, 2011
All Rights Reserved

DEXTRAL SHEAR AND NORTH-DIRECTED CRUSTAL SHORTENING
DEFINES THE TRANSITION BETWEEN EXTENSIONAL AND
CONTRACTIONAL PROVINCES IN NORTH-CENTRAL OREGON

by

Ajeet K Johnson

A THESIS

Submitted to

Oregon State University

in partial fulfillment of

the requirements for the

degree of

Master of Science

Presented January 18, 2011

Commencement June 2011

Master of Science thesis of Ajeet K Johnson presented on January 18, 2011.

APPROVED:

Major Professor, representing Geology

Chair of the Department of Geosciences

Dean of the Graduate School

I understand that my thesis will become part of the permanent collection of Oregon State University libraries. My signature below authorizes release of my thesis to any reader upon request.



Ajeet K Johnson, Author

ACKNOWLEDGMENTS

First and foremost, Andrew Meigs for having faith in my ability to accomplish something, even when I didn't, and for taking a chance on a somewhat dedicated, ski-bum for a graduate student. Without your encouragement, support and dedication to my projects (in education and life), I'm not sure I would have withstood grad school, thank you.

Many thanks go as well to many professorial types here at OSU whom have been influential and supportive throughout my graduate and undergraduate endeavors; Anita Grunder, John Dilles, Rob Harris, Roy Haggerty, et. al. Thanks for helping me stand tall when I was broken, literally and figuratively. Also a very special thank you to Robert Reynolds, my advisor when and where it all began in Central Oregon, for cultivating my interest in geology through your incredible dedication to hands-on geology! Above all, my field experiences are the ones where I thrived and learned the most so to all of you whom accompanied me in the field, I thank you immensely.

I would also like to acknowledge my friend network here at OSU for being both supportive and competitive enough to keep me going. Friends such as Mark Ford, Erin Lieuallen, Sara Alsbury, Lucian Farmer, Chris and Danielle. Many thanks to Justin, Katie and Sitka, for being my motivators, friends, **field assistants**, shoulders to cry on and physical support when I needed it (and I definitely needed it). Without all of you, I'd be huddled in a snow cave somewhere. Many thanks also to Matt Miller, Bruce Wagner and the folks of Dant and Tygh Valley for giving me support and shelter.

Of course I must thank many others who have supported my endeavors through the years, a few of which are; Katie and Chris (for an ever-open invitation to my sanctuary of Bend), Walter Mooney, Dave and Laura (for giving me confidence in myself) and all the students I've taught who have shown me how far I've come. Everyone who had a hand in educating me, as a TA, professor, or study-buddy, you ROCK!

Lastly, but FAR from least is my family, without whom I would not exist or be who I am. My parents for giving me their love and encouragement in everything I decide to do, whether it be snowboarding, tree-planting or grad school. You give my life meaning and I would be lost without your guidance and love. To Karen and Ron for supporting my life as a "Beaver" (and beyond) and to my grandmother, Elaine who is an inspiration for me to be a strong, intelligent woman, thank you a million times over.

TABLE OF CONTENTS

	<u>Page</u>
1. Introduction.....	1
2. Regional Tectonic Background.....	5
2.1 Regional tectonic rotation of the Cascade Forearc.....	5
2.2 Backarc Extension: Basin and Range.....	6
2.3 Backarc Contraction: Yakima fold belt.....	7
3. Methods.....	8
4. Tygh Valley Regional Stratigraphy.....	12
4.1 Oligocene Stratigraphy.....	17
4.2 Early Miocene Stratigraphy.....	18
4.3 Late Miocene to Pliocene Stratigraphy: Tygh Valley.....	21
4.4 Quaternary Sediments.....	23
5. South flank Tygh Valley: Mutton Mountain.....	24
5.1 Structural Relationships.....	24
5.2 Mutton Mountain structural model.....	26
5.3 Interpretation.....	28
6. North flank: Tygh Valley to Tygh Ridge.....	28
6.1 Structural Relationships.....	29
6.2 Faulting of Tygh Valley Sediments.....	34
6.3 Tygh Valley structural model.....	35
7. Regional structural model.....	37
7.1 Geodetic constraints on backarc deformation.....	39

TABLE OF CONTENTS (Continued)

	<u>Page</u>
7.2 Rate and time scale of deformation.....	42
8. Implications for a transition region.....	44
8.1 A structural model for backarc accommodation of clockwise rotation.....	45
8.2 Mutton Mountain and regional Oligocene volcanism.....	48
9. Conclusions.....	49
Bibliography.....	52

LIST OF FIGURES

<u>Figure</u>	<u>Page</u>
1: Tectonic Setting of Tygh Valley.....	2
2: Tygh Valley Regional Location Map.....	4
3: Dant and Maupin SW Geologic Maps.....	9
4: $^{40}\text{Ar}/^{39}\text{Ar}$ Age Spectra.....	10
5: Tygh Valley Stratigraphic Column.....	16
6: Dant and Maupin SW Cross-section.....	19
7: Cross-sectional View in Mutton Mountain.....	25
8: Tygh Valley Reconnaissance Geologic Map.....	30
9: Tygh Valley unconformities and faulting; A, B, C.....	31
10: Tygh Valley and Ridge image.....	32
11: Composite Regional Cross-Section of Tygh Valley.....	36
12: GPS velocity data comparison for the backarc.....	38
13: End Member Models for the Transition Region.....	41
14: Tectonic setting of the Transition Region.....	47

LIST OF TABLES

	<u>Page</u>
Table 1. $^{40}\text{Ar}/^{39}\text{Ar}$ Spectra.....	11
Table 2. Geochemical Comparison plots.....	13
Table 3. Geochemical Data.....	14

LIST OF APPENDICES

Page

Appendix A: Summary of $^{40}\text{Ar}/^{39}\text{Ar}$ Age Analyses:

JRB01 (Thrb).....	64
MMA01 (Tmi).....	65
MMD04 (Tmd).....	66
MMR02 (Tji).....	67
MMR04 (Tjr).....	68
TVF16 (Ttv ₂).....	69
TVF17 (Ttv ₁).....	70
TVF01 (Tnpb).....	71

Appendix B: XRF/ ICP-MS Analysis:

REE all basalts.....	72
REE Mutton Mountain.....	73
REE Tygh Valley basalts.....	74
Geochemical comparison of CRBG.....	75
Geochemical comparison of Mutton Mountain rhyolites.....	76
Geochemical comparison of Tygh Valley basalts.....	77

LIST OF PLATES

Plate

1. Geologic Map and cross-section of Dant Quadrangle
2. Geologic Map and cross-section of Maupin SW Quadrangle
3. Reconnaissance Geologic Map of Tygh Valley
4. Tygh Valley Regional Cross-section

Plates are located in the pocket at the back of the book.

1. Introduction

Active deformation of the North American plate in the Pacific Northwest reflects the influence of at least two tectonic processes. One process is northeast directed subduction of the Juan de Fuca plate beneath the North America plate and the other is clockwise rotation of the Oregon Coast Range (OCR) block with respect to stable North America (Hammond and Thatcher, 2005b; McCaffery et al., 2007; McCaffrey et al., 2000b; Wells et al., 1998) (Figure 1). Clockwise rotation of the OCR is expressed in the backarc as crustal extension in southeast Oregon and contraction in central Washington. Forearc rotation gives rise to extension in the backarc where rotation is directed away from the North American plate in the south and crustal shortening where rotation is directed toward the continent in the north.

Tectonically-driven clockwise rotation of the OCR forearc with respect to the North American plate is revealed in decadal timescales by GPS velocity data and on geologic timescales in paleomagnetic data (Magill et al., 1982; McCaffrey et al., 2007; Wells, 1990). Paleomagnetic data provide evidence for long-term rotation of the Cascade forearc block over a 10^6 timescale at a rate of $\pm 1.5^\circ/\text{m.y}$ (Magill et al., 1982; McCaffrey et al., 2007; Wells, 1990). These data show that contemporaneous motion of the forearc and deformation in the backarc are linked and have been for at least the last 11 Ma (Hammond and Thatcher, 2005b; McCaffery et al., 2007; McCaffrey et al., 2000b; Wells et al., 1998).

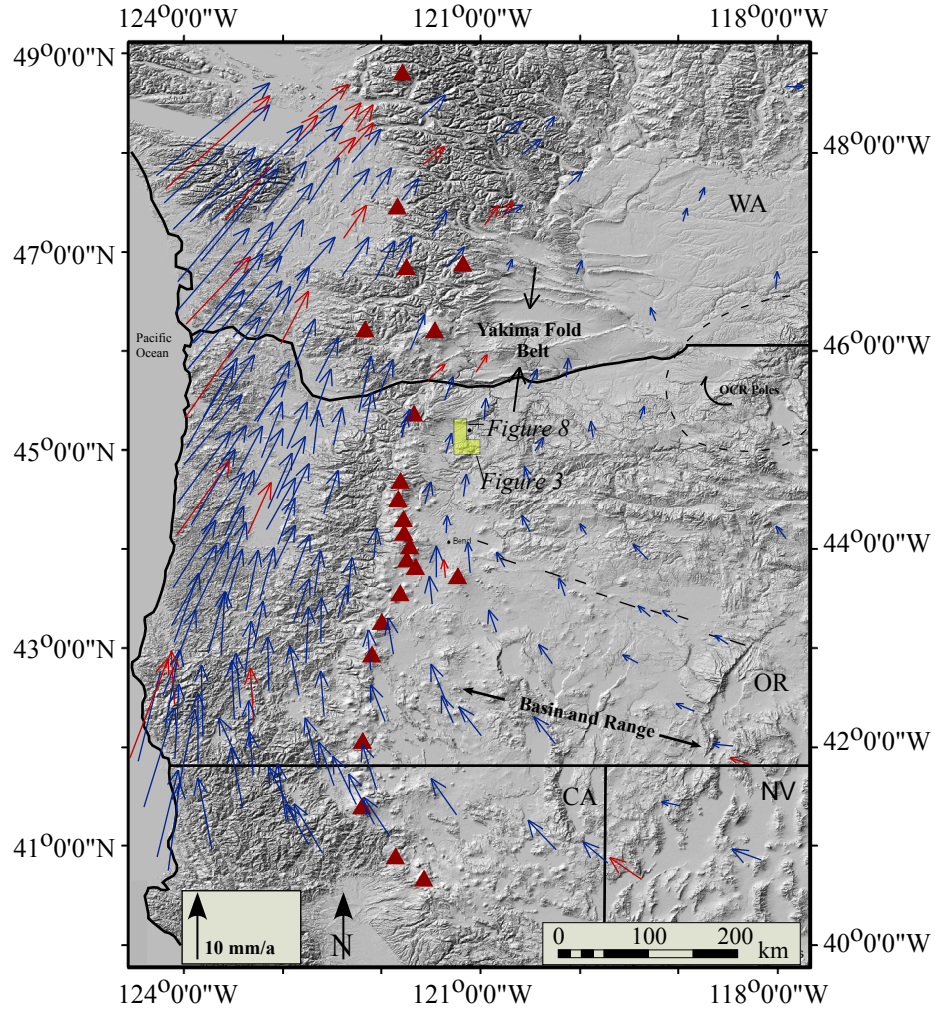


Figure 1. Regional tectonic map of the Pacific Northwest. Major physiographic and geologic provinces include the Cascade volcanic arc, the Basin and Range extensional province to the south of the brothers fault zone (dashed), the Yakima Fold belt, and the transition region (field study, yellow box). A dashed ellipse shows the range of proposed locations of the Oregon Coast Range block (OCR) rotational pole (Hammond and Thatcher, 2005; McCaffrey et al., 2000; McCaffrey et al., 2007; Wells et al., 1998) Arrows indicate GPS velocities relative to stable North America, arrow color defines the length of the survey (red, 10-15 yr; blue, 1-5 yr). Red triangles mark the location of individual volcanoes of the Cascade arc.

The observation that backarc deformation changes systematically from extension in the south to contraction in the north, requires that a transition occur between 43.5° and 45.5° N. Northwest-southeast directed Basin and Range extension is reflected by large northwest striking normal faults to the south of 44.5°N and terminates at the northern most fault of Green Ridge (Conrey, 1985; Pezzopane and Weldon, 1993b). To the north of 45.5° N, a series of east-trending folds and thrust faults reflects crustal shortening expressed in the Yakima Fold belt (Reidel et al., 1989a). Yakima Fold belt anticlinal folds change from northwest trending to northeast trending from south to north, respectively. Between 43.5°N and 45.0°, voluminous Pleistocene-Holocene basalts and sediments have resurfaced the landscape east of the high Cascades in the Deschutes, Tygh and Dalles basins, thereby obscuring structural relations in the transition region (Meigs et al., 2009; Smith, 1986a; Smith, 1986b).

In this study, I present a new model for regional structure and tectonics of north-central Oregon, based on new data from Tygh Valley, a structural low within the transitional region. This structural model for the Tygh Valley integrates new mapping and age data, GPS velocity data, and earthquake data. The purpose of this study is to understand the structural style, timing and rate of deformation of two broad wavelength structural highs, Tygh Ridge (north) and Mutton Mountain (south) in north-central Oregon (Figure 2). With these data I argue that folds related to east-west trending reverse faults are segmented by north-south trending strike-slip faults and mark a sharp boundary between the Basin and Range extensional faults and the Yakima Fold belt.

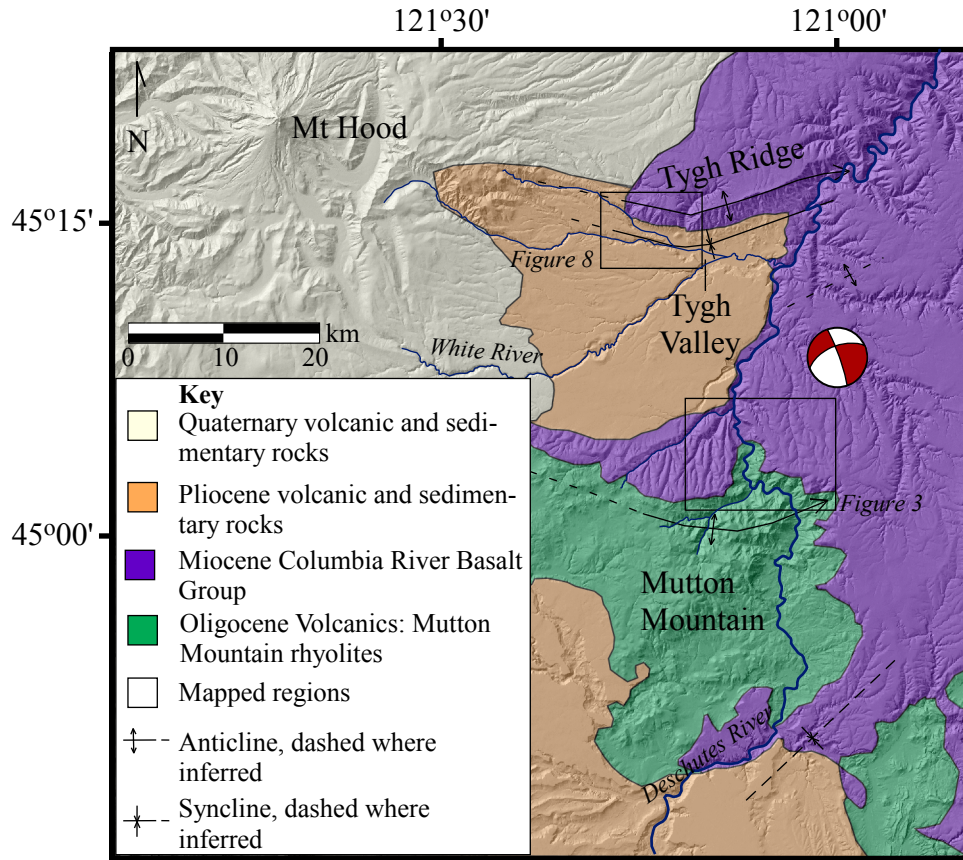


Figure 2. Location map of transition region and mapping areas (boxed). Features include the Tygh Ridge anticline, Tygh Valley syncline and Mutton Mountain anticline mapped during this study. A syncline axis south of Mutton Mountain is inferred based on data from Smith (1986). Beach ball diagram is representative of focal mechanisms resolved for local seismic events. Area covered by beach ball encompasses areal extent of most recent earthquakes.

In order to understand the structural controls, new stratigraphy, structural data and geochronologic data were analyzed and evaluated in concert with existing geodetic data. Since structures flanking Tygh Valley have good exposure of units from Oligocene to Quaternary in age, structural relationships are mapped with reasonable accuracy. A model for the transition region is defined as an abrupt change in crustal deformation from extension to contraction with a significant component of dextral shear between two stable blocks.

2. Regional Tectonic Background

Geographically, Tygh Valley is flanked by Mt. Hood to the west, the Deschutes River to the east, Tygh Ridge to the north and Mutton Mountain to the south. Geologically, the Tygh Valley lies in the backarc of the Cascadia subduction zone and related Cascade volcanic arc, where two opposing styles of crustal deformation; extension and contraction, appear to overlap (Figure 1). In December 2006 a swarm of earthquake activity began near the Tygh Valley. Over 420 earthquakes including a magnitude 4.2, were recorded by Earthscope's US Array and the Pacific Northwest Seismic Network (Braunmiller, et al. 2010).

2.1 Regional tectonic rotation of the Cascade Forearc

Northeast-directed subduction of the Juan de Fuca and related plates under the North American plate has generated arc volcanism since at least 45 Ma (Hammond and Thatcher, 2005a; McCaffrey et al., 2000a; McCaffrey et al., 2007; Wells, 1998). Deformation of the North American plate in the Pacific Northwest includes rigid body rotation of the Coast Range block in the forearc and distributed deformation in the

backarc. The approximate pole of rotation of the deformation field lies in the region of the Oregon-Washington-Idaho border (Hammond and Thatcher, 2005a; McCaffrey et al., 2000a; McCaffrey et al., 2007; Wells, 1998). Clockwise rotation about this pole help to explain east-west extension with respect to North America in the Basin and Range and the transition to north-south shortening in the Yakima Fold belt (Hammond and Thatcher, 2005a; Magill et al., 1982; McCaffrey et al., 2007; Pezzopane and Weldon, 1993a; Wells, 1998; Wells, 1990 ; Wells and Heller, 1988). Geodetic and paleomagnetic data imply that the Coast Range block rotates at rates of $\sim 1.5^\circ/\text{Ma}$ and translates northward at 3.5 to 9 mm/yr (Hammond and Thatcher, 2005a; McCaffrey et al., 2000a; McCaffrey et al., 2007; Wells, 1998). Total rotation of 16° for the Coast Range block suggests roughly 20-30% extension at a rate of about 10 mm/yr across the Basin and Range post 11 Ma (Figure 1)(Wells, 1998; Wells, 1990 ; Wells and Heller, 1988; Zoback et al., 1981). Summation of seismic moment tensor release and fault slip rates yields a lower ~ 4 mm/yr extension rate (Pezzopane and Weldon, 1993).

2.2 Backarc Extension: Basin and Range

Extensional faulting in the Basin and Range Province has been active since the mid Cenozoic (at least 30 Ma) (Christiansen et al., 1992; Hammond and Thatcher, 2005a; Heller et al., 1987; Lawrence, 1978), although the northwestern corner in south-central Oregon is younger than ~ 10 Ma (Meigs et al., 2009; Scarberry et al., 2009). Extensional faults throughout southeastern Oregon are active, but slow moving (Pezzopane and Weldon, 1993b). Basin and Range extension is defined by large N-S trending normal faults across the states of Oregon, eastern California, Nevada, Idaho

and Utah. Large normal faults in Oregon, with relief greater than 100 meters, include the Summer Lake, Abert Rim, Poker Jim Ridge, Hart Mountain, and Steens faults (Scarberry et al., 2009; Trench, 2008b). Fault scarps attest to the active normal faulting along the north-trending range fronts and a Holocene extension rate of up to 4 mm/yr, is observed but diminishes to the north (Pezzopane and Weldon, 1993b). The northwestern limit of Basin and Range style deformation is the Brothers Fault Zone (BFZ), a NW-SE trending shear zone extending from Bend, OR to the Steens Mountains in the SE corner of the state (Lawrence, 1976; Pezzopane and Weldon, 1993b; Scarberry et al., 2009; Trench, 2008b). Whereas the BFZ was originally thought to represent an intracontinental transform fault zone, limited strike-slip separation, down to the northeast normal separation, and fault tips of Basin and Range faults to the south, favor an interpretation of the BFZ as a down to the northeast extensional fault system (Meigs et al., 2009; Trench, 2008a).

2.4 Backarc Contraction: Yakima Fold Belt

The Yakima fold belt (YFB) shows north directed contraction in the backarc of central Washington. These folds have been active since at least 17 Ma and associated faults display evidence of seismic activity into the Holocene (Campbell and Bentley, 1981; Reidel et al., 1989a; West et al., 1996). In the YFB major asymmetrical anticlinal ridges characterize structure and are separated by synclinal valleys. Thickness variations within the Columbia River Basalt Group (CRBG) such as the Grande Ronde Member, suggest that the east-trending folds initially began to form in the early Miocene (16.5 Ma) (Reidel et al., 1989a). Thinning and pinch-out of CRBG

units at the crest of larger anticline ridges indicate that deformation and volcanism across the Columbia Plateau were coeval and allow constraints on rate of motion in the region (Reidel et al., 1989).

Crestal grabens, fault scarps, and exposures of young basalts that overlie Quaternary gravels indicate Quaternary fold growth in southern Washington (Campbell and Bentley, 1981; West et al., 1996). Seismicity, including a number of moderate earthquakes in the early 20th century and more recent activity at Toppenish Ridge also indicate that the region is actively deforming (Mann and Meyer, 1993).

3. Methods

Field geologic mapping focused on the Dant and Maupin SW 7.5' quadrangles (Figure 3). Rock samples were chosen from key stratigraphic units to determine age, geochemical composition, and regional correlations. These units include, from youngest to oldest, the basalts and basaltic andesites of Tygh Valley (Tnpb, Tjfb, Thrb, Tbc); Columbia River Basalt (CRBG), Grande Ronde Member; Prineville basalts; an andesitic intrusion (newly identified); and John Day Formation, Mutton Mountain rhyolites (newly identified) (McClaughry et al., 2009; Smith, 1986b; Smith et al., 1987). Samples and points of observation were located through use of a Garmin eTrex GPS unit. Key stratigraphic units, including the John Day Formation (36-18 Ma), Columbia River Basalts Grande Ronde Member (16-14.5 Ma), Deschutes Formation (8.5-4.5 Ma), and the Juniper Flats basalt (2.6 Ma) were dated using a combination of ⁴⁰Ar/³⁹Ar dating (Figure 4, Table 1) and correlation via geochemical

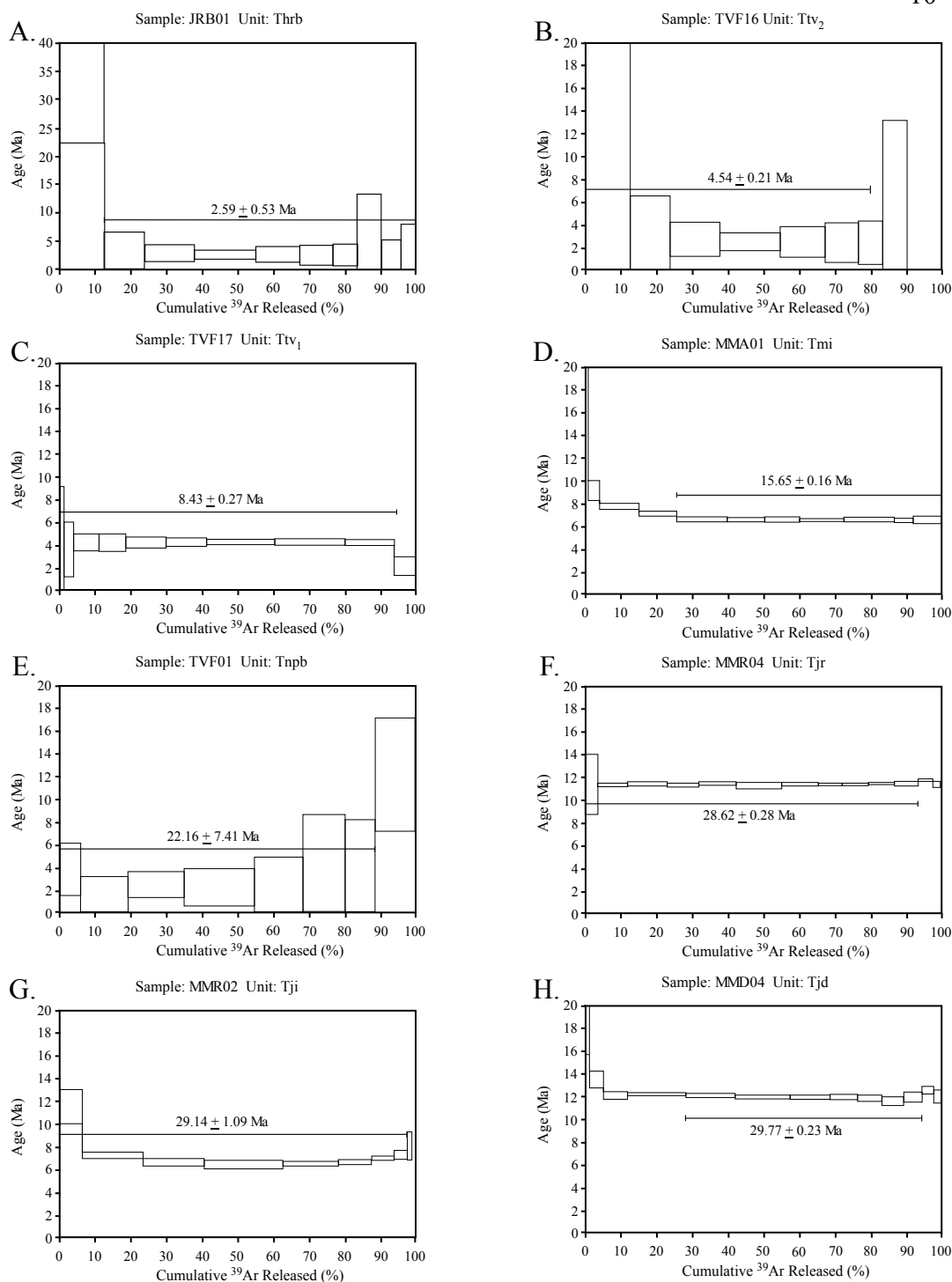


Figure 4. $^{40}\text{Ar}/^{39}\text{Ar}$ age spectra for units Ttv₂ (A. TVF16), Tji (B. MMR02), Tmi (C. MMA01), Tjr (D. MMR04), Tjd (E. MMD04), Ttv₁ (F. TVF17), Tnpb (G. TVF01), Thrb (H. JRB01). All age data were used except for Tnpb as the sample contained high atmospheric Argon. See Table 3.

Table 1. $^{40}\text{Ar}/^{39}\text{Ar}$ Age results for samples collected

Sample No.	Latitude	Longitude	Rock location/type	Material Dated	Analysis	Steps	% ^{39}Ar	K/Ca	Age $\pm 2\sigma$ (Ma)	Sample No.	Analysis	K/Ca	Age $\pm 2\sigma$ (Ma)
AKJ TVF-01 (Tnpb)	45° 06'07.00"N	121°10'28.20"W	Natural Pasture Basalt	Plagioclase	weighted plateau	8	88.65	0.005	22.16 \pm 7.41	AKJ TVF-01 (Tnpb)	Total Fusion Age	0.01	31.40 \pm 13.02
AKJ TVF-05 (Tnpb)	45°15'48.64" N	121°15'06.10"W	Juniper Flats-Basalt	Groundmass	weighted plateau	8	60.81	0.04	0.49 \pm 2.08	AKJ TVF-05 (Tnpb)	Total Fusion Age	0.04	3.72 \pm 1.74
AKJ MMR-04 (Tjr)	45°04'09.46"N	121°06'31.87"W	Mutton Mountain-Pumice	Glass	weighted plateau	13	93.98	2.838	28.62 \pm 0.28	AKJ MMR-04 (Tjr)	Total Fusion Age	6.05	28.58 \pm 0.29
AKJ MMR-02 (Tji)	45°02'39.13"N	121°03'38.95"W	Mutton Mountain-Rhyolite	Plagioclase	Isochron	6	88.59	6.96	29.14 \pm 1.09	AKJ MMR-02 (Tji)	Total Fusion Age	6.79	34.43 \pm 0.76
AKJ MMA-01 (Tmi)	45°02'06.58"N	121°05'09.22"W	Mutton Mountain-Andesite	Groundmass	weighted plateau	11	73.93	0.26	15.65 \pm 0.16	AKJ MMA-01 (Tmi)	Total Fusion Age	0.4	5.51 \pm 0.06
AKJ MMD-04 (Tjd)	45°02'32.08"N	121°06'16.81"W	Mutton Mountain-Rhyolite	Plagioclase	weighted plateau	14	66.52	0.21	29.77 \pm 0.23	AKJ MMD-04 (Tjd)	Total Fusion Age	0.25	9.89 \pm 0.06
AKJ TVF 16 (Ttv1)	45°14'26.14" N	121°11'32.06"W	Tygh Valley-Pumice	Glass	weighted plateau	8	79.8	0.83	4.54 \pm 0.21	AKJ TVF 16 (Ttv1)	Total Fusion Age	0.6	5.35 \pm 0.21
AKJ TVF 17 (Ttv2)	45°15'29.94" N	121°13'50.54"W	Tygh Valley-Pumice	Glass	weighted plateau	10	93.79	0.02	8.43 \pm 0.27	AKJ TVF 17 (Ttv2)	Total Fusion Age	0.02	8.13 \pm 0.34
AKJ TVA03 (Thrb)	45°07'48.64" N	121°10'30.12"W	Juniper Flats-Andesite	Groundmass	weighted plateau	10	87.53	0.01	2.59 \pm 0.53	AKJ TVA03 (Thrb)	Total Fusion Age	0.01	8.26 \pm 3.26

“fingerprinting” (Table 2) (Conrey, 1985; Hooper et al., 1993; McClaughry et al., 2009; Reidel et al., 1989b; Robinson, 1973; Smith, 1986b; Taylor, 1973).

Samples for dating and geochemical analysis were crushed using an alumina jaw crusher and clean, pea-sized fragments were hand picked and soaked in dilute HCl to remove traces of CaCO₃. Samples were washed thoroughly with de-ionized H₂O, dried at low temperature prior to shipment to the Washington State University GeoAnalytical Laboratory for XRF and ICP-MS analysis (Johnson et al., 1999).

Whole rock samples were analyzed for chemical compositions at Washington State and trace elements were analyzed by ICP-MS (Table 3). Age dates (⁴⁰Ar/³⁹Ar) were done at Oregon State University Noble Gas Mass Spectrometry lab in the College of Oceanic University’s analytical lab¹. Major elements were analyzed using XRF while minor and Atmosphere Sciences. Geochemical composition was used to fingerprint samples and correlate with the CRBG Grande Ronde Member, Prineville basalts, Deschutes and John Day Formations. Fingerprinting allowed for correlation of map units with previously published units such as the Columbia River Basalt, Prineville basalt (Hooper et al., 1993) and correlation of Mutton Mountain rhyolites with those of Gray Butte (Smith et al., 1998) (Table 2).

4. Tygh Valley Regional Stratigraphic Sequence

Figure 5 shows a generalized stratigraphic column for Tygh Valley.

Geochemistry and ⁴⁰Ar/³⁹Ar data are presented in Table 1. Oligocene units exposed in Mutton Mountain, yield ages that vary from 28.5-29.7 Ma (Figure 5, Table 1).

¹ For detailed analysis process, see WSU Analytical lab website: <http://www.sees.wsu.edu/Geolab/index.html>

Table 2. Geochemical Classification Diagrams

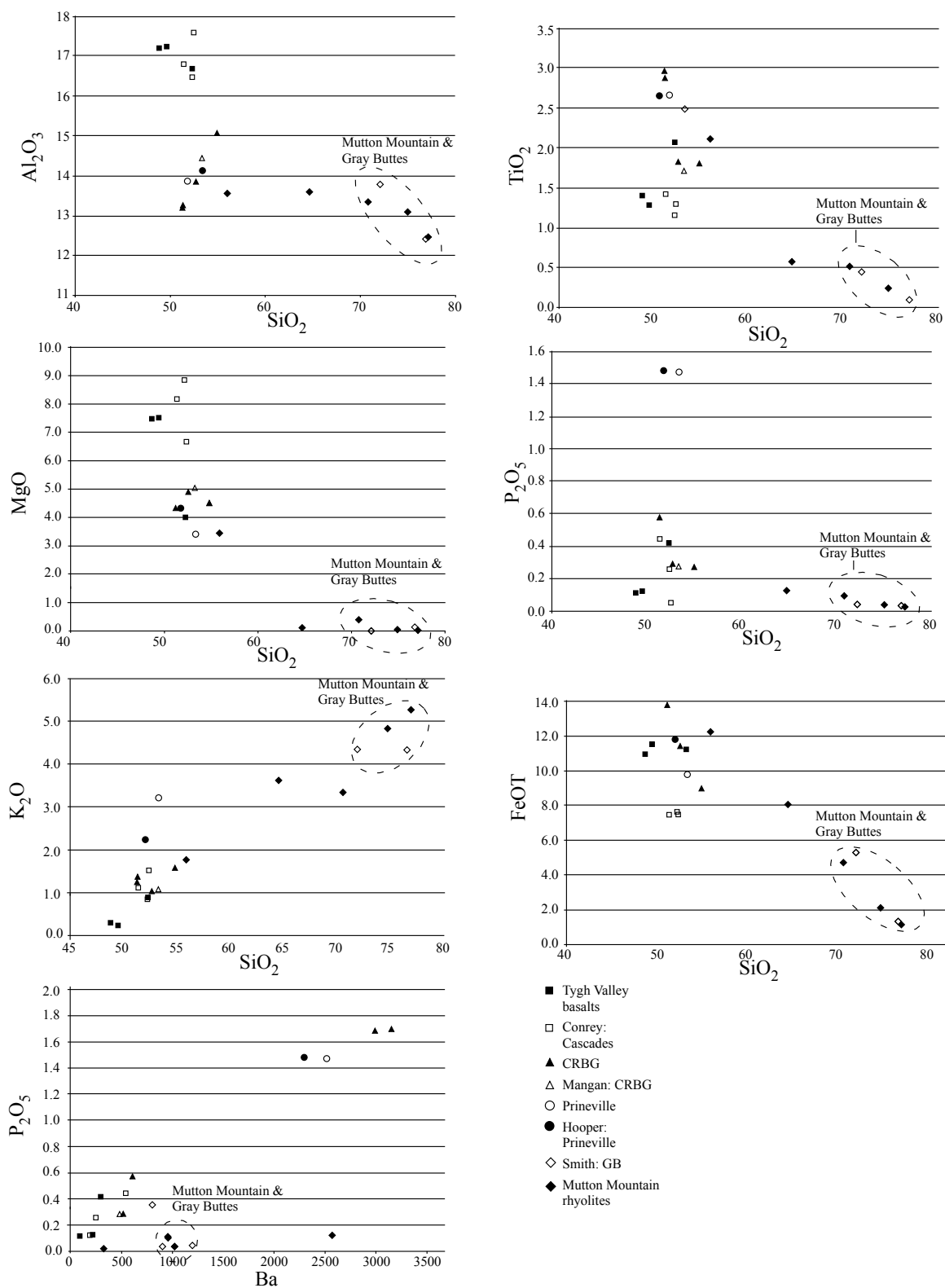


Table 3. Geochemical Analysis

	AKJ MMR-04	AKJ MMR-02	AKJ MMA-01	AKJ MMD-04	AKJ TVF-05	AKJ TVF-01	AKJ TVA-03	AKJ TVB-01	AKJ TGR-02	AKJ MMB-01 (Prineville)	AKJ MMR02R
Date	5-Apr-10	5-Apr-10									
	Tjr	Tji	Tmi	Tjd	Tjfb	Tjfb	Thrb	Tgr	Tgr	Tgr (Prineville)	Tji
Unnormalized Major Elements (Weight %):											
SiO ₂	73.05	76.06	55.51	68.93	49.56	48.79	52.28	51.30	52.70	53.38	75.97
TiO ₂	0.23	0.09	2.10	0.51	1.28	1.40	2.07	2.87	1.83	2.49	0.10
Al ₂ O ₃	12.74	12.28	13.44	13.00	17.23	17.20	16.67	13.19	13.85	14.12	12.31
FeO*	2.02	1.12	12.11	4.63	11.53	10.98	9.96	13.79	11.47	9.80	1.14
MnO	0.02	0.02	0.20	0.09	0.18	0.18	0.16	0.22	0.22	0.22	0.02
MgO	0.05	0.03	3.42	0.33	7.51	7.49	4.00	4.32	4.92	3.39	0.05
CaO	0.76	0.63	6.96	2.15	9.67	9.50	8.50	8.25	8.91	6.33	0.64
Na ₂ O	3.82	3.16	3.29	4.42	3.07	2.82	3.81	2.85	2.79	3.69	3.18
K ₂ O	4.70	5.17	1.75	3.26	0.25	0.30	0.89	1.36	1.02	3.21	5.17
P ₂ O ₅	0.04	0.02	0.36	0.09	0.12	0.12	0.42	0.58	0.29	1.47	0.02
Sum	97.43	98.59	99.13	97.40	100.41	98.78	98.76	98.72	98.00	98.09	98.59
Normalized Major Elements (Weight %):											
SiO ₂	74.97	77.15	55.99	70.77	49.36	49.39	52.93	51.97	53.77	54.42	77.06
TiO ₂	0.24	0.09	2.12	0.52	1.27	1.42	2.09	2.91	1.87	2.54	0.10
Al ₂ O ₃	13.08	12.46	13.56	13.34	17.16	17.41	16.88	13.36	14.14	14.39	12.48
FeO*	2.08	1.14	12.22	4.75	11.48	11.11	10.09	13.97	11.70	9.99	1.16
MnO	0.02	0.02	0.20	0.09	0.18	0.18	0.16	0.22	0.22	0.22	0.02
MgO	0.05	0.03	3.45	0.34	7.48	7.58	4.05	4.38	5.03	3.45	0.05
CaO	0.78	0.64	7.02	2.21	9.63	9.62	8.61	8.36	9.10	6.45	0.65
Na ₂ O	3.92	3.21	3.32	4.54	3.06	2.86	3.85	2.89	2.85	3.76	3.22
K ₂ O	4.82	5.25	1.77	3.35	0.25	0.30	0.90	1.37	1.04	3.27	5.24
P ₂ O ₅	0.04	0.02	0.36	0.10	0.12	0.12	0.43	0.58	0.29	1.50	0.02
Total	100.00	100.00	100.00	100.00	100.00	100.00	100.00	100.00	100.00	100.00	100.00
Unnormalized Trace Elements (ppm):											
Ni	3.80	3.70	14.50	4.70	114.80	118.10	21.20	19.20	17.80	17.80	2.50
Cr	3.10	3.90	4.60	5.00	180.30	195.50	45.10	38.60	38.30	5.00	2.90
Unnormalized Trace Elements (ppm), continued:											
Sc	6.40	2.30	33.20	12.60	29.70	32.70	25.10	36.50	35.40	34.50	2.40
V	4.20	5.10	361.70	21.20	195.50	206.40	212.80	407.00	323.40	239.50	5.00
Ba	918.10	289.70	712.80	856.70	192.60	75.00	265.70	576.80	471.20	2255.60	292.00
Rb	132.00	185.50	51.10	108.70	3.30	2.00	13.80	33.40	22.60	44.50	185.80
Sr	68.00	26.70	311.90	120.00	285.70	649.00	510.20	317.60	323.90	299.30	27.40
Zr	471.50	118.30	190.30	626.80	75.50	76.40	147.50	200.30	153.30	137.30	117.00
Y	41.30	42.20	37.30	68.00	24.50	23.30	26.80	42.10	32.90	50.40	42.20
Nb	29.30	20.40	13.70	31.80	5.60	5.50	13.80	16.20	12.00	9.10	19.60
Ga	24.50	22.90	21.90	24.80	18.30	18.00	20.70	21.70	21.70	19.50	22.00
Cu	4.10	5.80	24.20	7.70	46.90	55.50	41.50	28.10	31.80	28.20	5.30
Zn	95.50	46.30	126.70	120.20	87.90	86.40	100.00	143.30	114.90	121.10	47.70
Pb	16.00	21.00	9.90	13.80	1.80	0.60	2.50	5.80	6.00	7.40	20.00
La	53.20	38.30	23.20	54.40	10.30	2.50	16.10	27.10	19.10	26.80	38.60
Ce	94.20	68.50	52.00	110.80	15.40	15.20	38.70	59.50	42.00	59.50	73.40
Th	13.80	20.10	6.30	10.90	0.00	0.00	1.70	3.80	2.10	2.90	20.30
Nd	51.70	30.20	28.50	54.30	10.30	10.40	23.10	33.60	23.90	42.20	32.70
U	2.70	6.90	2.50	3.50	1.50	0.30	0.60	1.30	0.40	2.70	5.60

Table 3. Geochemical Analysis

	AKJ MMR-04	AKJ MMR-02	AKJ MMA-01	AKJ MMD-04	AKJ TVF-05	AKJ TVF-01	AKJ TVA-03	AKJ TVB-01	AKJ TGR-02	AKJ MMB-01	AKJ MMR02R
	Tjr	Tji	Tmi	Tjd	Tjfb	Tjfb	Thrb	Tgr	Tgr	Tgr (Prineville)	Tji
sum tr.	2033.40	957.80	2026.30	2255.90	1299.90	1572.80	1526.90	2011.90	1692.70	3403.30	962.40
in %	0.20	0.10	0.20	0.23	0.13	0.16	0.15	0.20	0.17	0.34	0.10
mm m+tr	97.64	98.68	99.33	97.63	100.54	98.94	98.91	98.92	98.17	98.43	98.68
+Toxides	97.68	98.70	99.38	97.68	100.57	98.98	98.95	98.97	98.21	98.49	98.70
Major elements are normalized on a volatile-free basis, with total Fe expressed as FeO.											
NiO	4.84	4.71	18.45	5.98	146.09	150.29	26.98	24.43	22.65	22.65	3.18
Cr2O3	4.53	5.70	6.72	7.31	263.52	285.74	65.92	56.42	55.98	7.31	4.24
Sc2O3	9.82	3.53	50.92	19.33	45.56	50.16	38.50	55.99	54.30	52.92	3.68
V2O3	6.18	7.50	532.11	31.19	287.60	303.64	313.06	598.75	475.76	352.33	7.36
BaO	1025.06	323.45	795.84	956.50	215.04	83.74	296.65	644.00	526.09	2518.38	326.02
Rb2O	144.36	202.86	55.88	118.87	3.61	2.19	15.09	36.53	24.72	48.67	203.19
SrO	80.42	31.58	368.86	141.91	337.87	767.51	603.37	375.60	383.05	353.95	32.40
ZrO	636.90	159.80	257.06	846.68	101.99	103.20	199.24	270.57	207.08	185.46	158.04
Y2O3	52.45	53.59	47.37	86.36	31.11	29.59	34.03	53.46	41.78	64.01	53.59
Nb2O5	41.91	29.18	19.60	45.49	8.01	7.87	19.74	23.17	17.17	13.02	28.04
Ga2O3	32.93	30.78	29.44	33.34	24.60	24.20	27.83	29.17	29.17	26.21	29.57
CuO	5.13	7.26	30.29	9.64	58.71	69.47	51.95	35.18	39.81	35.30	6.63
ZnO	119.61	57.99	158.69	150.55	110.09	108.21	125.25	179.48	143.91	151.68	59.74
PbO	17.24	22.62	10.66	14.87	1.94	0.65	2.69	6.25	6.46	7.97	21.54
La2O3	62.39	44.92	27.21	63.80	12.08	2.93	18.88	31.78	22.40	31.43	45.27
CeO2	115.80	84.20	63.92	136.20	18.93	18.68	47.57	73.14	51.63	73.14	90.23
ThO2	15.23	22.18	6.95	12.03	0.00	0.00	1.88	4.19	2.32	3.20	22.40
Nd2O3	60.30	35.22	33.24	63.33	12.01	12.13	26.94	39.19	27.88	49.22	38.14
U2O3	2.97	7.60	2.75	3.85	1.65	0.33	0.66	1.43	0.44	2.97	6.16
Cs2O	0.00	0.00	0.00	0.00	0.00	0.00	0.00	0.00	0.00	0.00	0.00
As2O5	0.00	0.00	0.00	0.00	0.00	0.00	0.00	0.00	0.00	0.00	0.00
W2O3	0.00	0.00	0.00	0.00	0.00	0.00	0.00	0.00	0.00	0.00	0.00
sum tr.	2438.06	1134.68	2515.97	2747.23	1680.41	2020.52	1916.23	2538.72	2132.58	3999.82	1139.44
in %	0.24	0.11	0.25	0.27	0.17	0.20	0.19	0.25	0.21	0.40	0.11

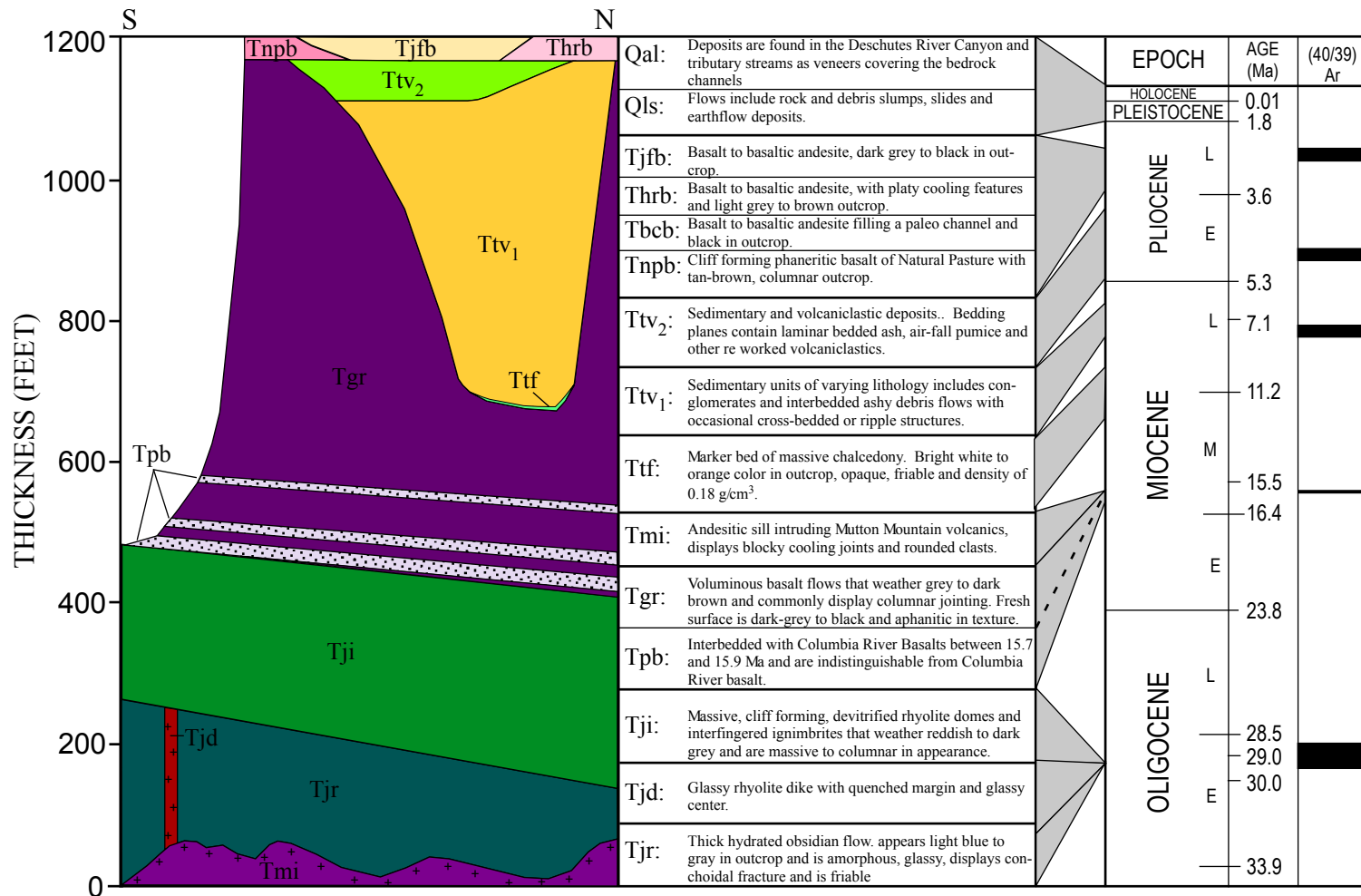


Figure 5. Generalized stratigraphic column for Mutton Mountain, Tygh Ridge, and Tygh Valley. Relative thickness, age and stratigraphic relationships based on data in this study. Age data are presented in Table 1. Brief unit descriptions and correlating age data are included.

Columbia River Basalt Group units were lumped together as a single map unit based on field observations and because the different members were indistinguishable in hand sample. Tygh Valley Formation of the late Miocene-Pliocene (Bela, 1982; Conrey, 1985; Farooqui et al., 1981; Smith et al., 1987) was subdivided into three sedimentary packages and three basalt flows. Together the age and structural relationships of units within the Tygh Valley Formation serve to delineate depositional settings and constrain the timing of deformation. All $^{40}\text{Ar}/^{39}\text{Ar}$ dates given are new data unless otherwise indicated by parentheses, followed by references cited.

4.1 Mutton Mountain Rhyolite Complex (Oligocene):

Mutton Mountain Obsidian flow (Tjr) (Figure 4 & 5, Table 1, 2 & 3)

Comprised of a thick (263m) hydrated obsidian this unit is glassy with conchoidal fracture near contacts with other units. Near the center of the unit it is more solid and less hydrated. Less resistant to weathering, this hydrated obsidian often forms slopes, appears light blue to grey in outcrop, is aphyric, glassy, and is friable. The lower contact with older Clarno Formation is irregular and only exposed in lower canyon walls. The upper contact with rhyolite is marked by a thick sequence of flow breccia containing hydrated obsidian, pumice and rhyolite clasts (1mm to >5m) with occasional angular lithic clasts. Both this unit and the older Clarno Formation are cut by a 29.77 ± 0.23 Ma Oligocene dike. $^{40}\text{Ar}/^{39}\text{Ar}$ age dating revealed an age for this unit younger than overlying units. This discrepancy is attributed to potassium loss and atmospheric argon contamination of the glass. The structural relationships of Tjr with Tji and Tjd, indicate Tjr is the older of the Mutton Mountain volcanic units.

Tertiary rhyolite dike (Tjd) (Figure 4 & 5, Table 1 & 3) A 29.77 ± 0.23 Ma dike cuts Tjr and is characterized by sharp, glassy quenched margins that bound its width between 1.5-9 m. Tjd contacts with Tjr strike northwest (309°) and dip steeply (88°) (Figure 6). The center portion is dense glassy rhyolite, tan to white in color with common light grey to black bands of obsidian near its quenched margin.

Mutton Mountain Rhyolite (Tji) (Figure 4 & 5, Table 1, 2 & 3) Both the upper and lower contacts of these rhyolite flows with Tgr and Tjr, respectively, are irregular surfaces. The lower contact with Tjr obsidian is sharp, overlying obsidian flow breccia and the upper contact with overlying Grande Ronde Member of CRBG and Prineville basalts is disconformable (Figure 6). This rhyolite unit forms the majority of outcrop within the Mutton Mountains and comprises massive, cliff forming, devitrified flows, up to 224 m thick, with inter-fingered ignimbrites. Outcrops weather reddish to dark grey and are massive to columnar in appearance with no apparent cleavage pattern at outcrop or hand sample scale. Geochemically and chronologically, the 29.14 ± 1.09 Ma rhyolites of Mutton Mountain correlate with Gray Butte rhyolites (28.82 ± 0.23 Ma) of Smith et. al (1998) to the southeast (Table 2).

4.2 Columbia River Basalt Group; Grande Ronde Member:

The landscape of north central Oregon is dominated by gentle rolling hills of basalt. Most mappable outcrops here are Columbia River Basalt Group, which cover $163,700 \text{ km}^2$ in southern Washington, northern Oregon and western Idaho and are between 17.5-14 Ma (Reidel, 1983; Reidel et al., 2003; Robinson, 1973; Tolan et al., 1989). The most voluminous and widespread unit is the Grande Ronde Member,

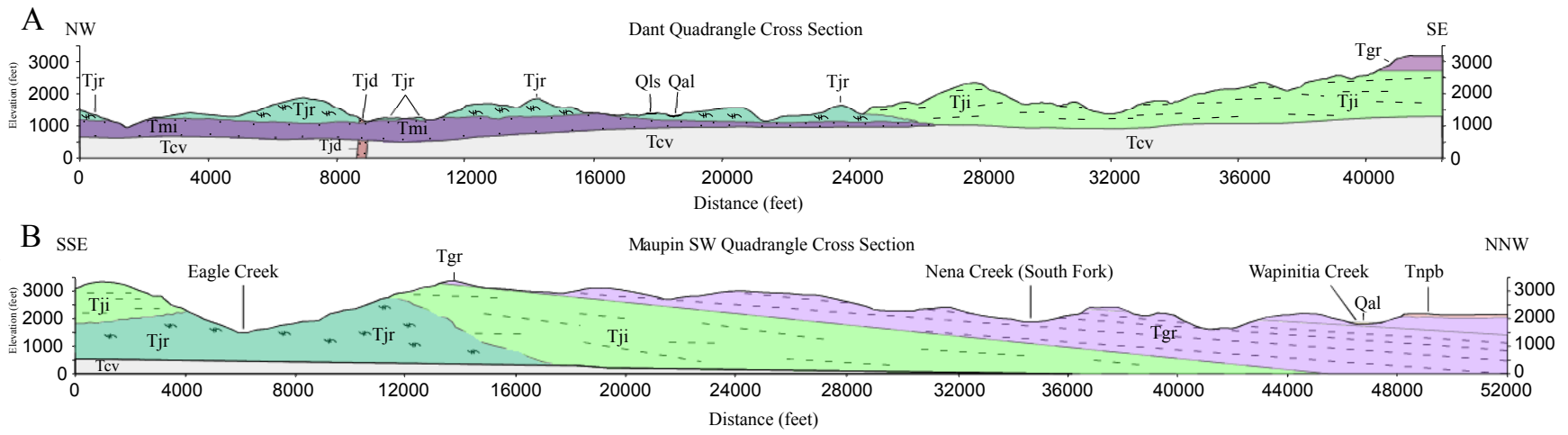


Figure 6. Cross sections for Dant (A, upper) and Maupin SW (B, lower) quadrangles. Note onlap of Mutton Mountain rhyolite dome complex by the Columbia River Basalt Group flows in B. Plus symbols represent an intrusive contact.

which has an approximate volume of 148,600 km³ (Reidel, 1983; Reidel et al., 1989b; Tolan et al., 1989). CRBG flows in the field are nearly indistinguishable from one another in hand sample and can only be separated into individual units on the basis of geochemistry. Geochemical data indicates that units in Tygh Valley are part of the Grand Ronde Member, particularly the Winter Water flow (15.7-15.6 Ma) and the N₂ flows, (≥ 15.9 Ma) (Table 2) (Hooper et al., 1993; Reidel et al., 1989b). Basalts of the CRBG interfinger locally with Prineville basalts that are indistinguishable in hand sample. Some investigators include the Prineville basalt in the CRBG whereas others infer they are unrelated due to their unique geochemical signatures. Prineville basalts have high P₂O₅/SiO₂ content making them geochemically distinct, a characteristic that defines Prineville basalts from the Grand Ronde member in central Oregon (Table 2) (Hooper et al., 1993; Uppuluri, 1974).

Columbia River Basalt Group; Grande Ronde Member (Tgr) (Figure 4 & 5, Table 2 & 3) Thick flows of the CRBG display well formed columns and entablature near the center of flows (Reidel et al., 2003; Reidel et al., 1989b). Individual flows are distinguished by vesiculation in the uppermost part of the flow. Fresh surfaces are dark-grey to black and aphanitic in texture with only sparse micro-phenocrysts of plagioclase evident without hand-lens. Prineville basalts interfinger with the Columbia River Basalts and are between 15.7 to 15.9 Ma (Hooper et al., 1993; Uppuluri, 1974). Prineville basalt flows average 9-18 m thick locally (15.7-15.6 Ma; ≥ 15.9 (Hooper et al., 1993; Mangan et al., 1986; Reidel et al., 1989b; Uppuluri, 1974) Ma).

Miocene Mutton Mountain Intrusion (Tmi) (Figure 4 & 5, Table 1 & 3) A

15.65±0.16 Ma andesitic sill, ~30 m thick, crops out within the Deschutes River canyon below Tjr (Oligocene) (Figure 5 & 6). Exposures display blocky cooling features with abundant, rounded, mafic, xenocrysts (2-6 cm). Fresh surfaces are matte black, have a microcrystalline groundmass and contain sparse phenocrysts of weathered pyroxene, olivine, and fractured plagioclase.

4.3 Tygh Valley Formation (Late Miocene to Pliocene)

Units overlying the Columbia River Basalts are restricted to the center and margins of Tygh Valley. Post-Miocene sediments are volcanoclastic sandstones and conglomerates and other sedimentary deposits associated with the Deschutes and Tygh Valley Formations as described by Smith (1986b, 1987), Conrey (1985), Robinson (1973) and Farooqui (1981). Sediment sources include drainage off the developing high Cascade volcanic arc to the west (O'Connor et al., 2002; Taylor, 1973) and the mountainous terrane bounding the basin on the north, south and east.

Tygh Valley chalcendony (Ttf) (Figure 5) This unit is a distinctive bed of silicic material cropping out along the south flank of Tygh Ridge. It overlies older CRBG and is overlain by younger sedimentary and volcanoclastic strata of the Tygh Valley Formation (Farooqui et al., 1981; O'Connor et al., 2002; Smith, 1986a; Smith et al., 1987). Averaging ~3 m in thickness, the chalcedony is massive, has a bright white to bright orange color, is opaque, is brittle and contains sparse fragments of petrified wood. Secondary fractures are filled with dark grey, semi-translucent quartz.

Tygh Valley volcanoclastic sediments (Ttv₁) (Figure 4 & 5, Table 1) This sedimentary package has an age of $\sim 8.43 \pm 0.27$ Ma near its upper contact with Ttv₂, contains clasts of varying composition derived from the Cascade arc and local sources. The unit is approximately 1000 m thick and locally composed of conglomerates, sandstones and ashy debris flows (lahars) displaying flow indicators such as normal and reverse grading, laminar or cross-bedding and climbing ripples.

Tygh Valley volcanoclastics (Ttv₂) (Figure 4 & 5, Table 1) Sediments derived from the Cascade arc unconformably overlying Ttv₁ and comprise a second package of volcanoclastic strata and are $\sim 4.54 \pm 0.21$ Ma, near the basal contact with Ttv₁. Planar bedded air-fall ash, pumice and other reworked volcanoclastic material predominate. Volcanoclastics are typically very fine to coarse grained, reversely graded with white, red, green and black bed colors.

Natural Pasture basalt (Tnpb) (Figure 4 & 5, Table 1, 2 & 3) The basalt of Natural Pasture and southern Juniper Flat is a cliff forming basalt that averages ± 30 m thick. This basalt appears to fill a paleo-channel incised into the CRBG, the flow(s) thicken to >30 m and thin to <10 m within 50 m (Figure 5). Outcrops are blocky, flat lying, tan-brown and columnar, with a light grey to almost purple fresh surface. A fine-grained and equigranular groundmass encases common, large, phenocrysts of olivine weathered to iddingsite and plagioclase. The light grey color and abundance of phenocrysts differentiates this unit from basalts of the CRBG.

Happy Ridge basalt (Thrb) (Figure 4 & 5, Table 1, 2 & 3) Happy Ridge basalt crops out near the southern limb of Tygh Ridge as a flat-lying lava flow. Happy Ridge is a

basaltic andesite flows within the Tygh Valley Formation of Smith (1987). This basalt overlies the Tygh Valley sediments of Tv_{f1} and has an age of 2.59 ± 0.53 Ma. In outcrop as well as in hand sample, Happy Ridge displays platy cooling features, weathers light grey to brown and has a flow thickness, between 10m and >25 m.

Juniper Flats basalt (Tjfb) (Figure 5) Juniper Flats lava is a basalt to basaltic andesite that forms a flat-lying, cliff-forming unit to the south and west on Juniper Flats and is one of several lava flows of the Tygh Valley and Deschutes Formations of Smith (1987) and Farooqui (1981). Flow(s) of Juniper Flat appear to mark an angular unconformity with Tv_{f1} and thicken from ~10 m to >30 m toward the south. Outcrops are dark grey to black, scoriaceous, 10-20m thick and display poorly developed columnar jointing in the center of the thickest flow sections.

Badger Creek basalts (Tbcb) (Figure 5) The Badger Creek basalt appears to be a channel filling flow or an eruptive center, however, limited contact exposure and extensive landslide debris make the nature of this contact difficult to determine. Badger Creek channel is the place where this basalt crops out. It is black with clinker texture, very thick (≥ 60 m), and lacks flow indicators. Fresh surfaces are black, have porphyritic texture and are heavily vesiculated ($>50\%$, ≥ 3 mm).

4.4 Quaternary sediments:

Quaternary Landslide deposits (Qls) Landslides are an unconsolidated, poorly sorted mixture of basaltic, rhyolitic, tuffaceous “blocks”. Earth flows include rock and debris slumps, slides and contain abundant large boulders and intact bedrock blocks that preserve original stratigraphic relationships. The largest deposits originate at the

contact of the Grande Ronde Member and the John Day Formation along the Deschutes River Canyon.

Quaternary Alluvium (Qal) Composition of local alluvium ranges from clasts of rhyolite to basalts. Deposits are found in the Deschutes River Canyon and tributary streams as unconsolidated veneers mantling bedrock.

5. South flank Tygh Valley: Mutton Mountain

A gently north-sloping panel of Columbia River Basalts (CRBG) unconformably overlying the Mutton Mountain rhyolite complex dominates the landscape on the south flank of Tygh Valley. Deformation associated with long wavelength folding continues to 5 km south of Mutton Mountain where a NE trending syncline of CRBG dissipates at Gateway, Oregon (Smith, 1986b).

5.1 Structural Relationships

Mutton Mountain is a topographic high standing ~1000 m in elevation. To the east, Mutton Mountain is bounded by the Deschutes River, which exploited the contact between Miocene Columbia River Basalt Group and the Oligocene Mutton Mountain rhyolites (Figure 6). Contact and structural relationships between the Mutton Mountain rhyolite units and CRBG are revealed along the Deschutes River canyon where the river has incised over 610 m. (Figure 6 & 7).

The ~28.5 Ma, Mutton Mountain obsidian flow lies at the bottom of the Deschutes River canyon. Weak obsidian (Tjr) and irregular contacts with the overlying Tji result in incompetent outcrops where orientation measurements are not reliable. Outcrop characteristics suggest a northeast dip because internal contacts lose

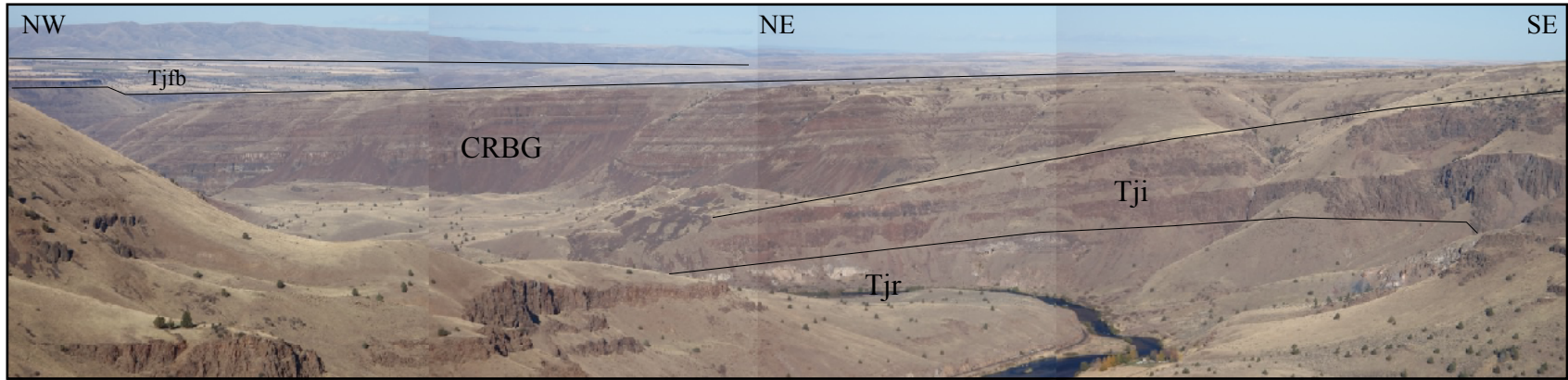


Figure 7. Panoramic view looking NE across the Deschutes River canyon (foreground) near Dant, OR.

elevation from south to north (Figures 5, 6 & 7). Conformably overlying the Mutton Mountain obsidian are Mutton Mountain rhyolite flows (Tji), which dip between 06° and 15° to the NE (Figure 3 & 6).

The package of multiple CRBG flows thickens from south to north (>15 flows) and pinches out to the south (1-2 flows) against the northern flank of Mutton Mountain, west of the Deschutes River. A consistent 06° NE dip characterizes the CRBG north of the summit of Mutton Mountain. East of the Deschutes River, at the same latitude, CRBG thin but are continuous farther south where Smith (1986b) noted a change to south dip (Figure 3 & 6). Thus the south flank of Mutton Mountain comprises the northwest limb of the northeast trending Gateway syncline at $\sim 44^{\circ}50'30''\text{N}$, $121^{\circ}01'12.5''\text{W}$.

Immediately north of Mutton Mountain, the CRBG package thickens to >300 m, but maintains its $\sim 6^{\circ}$ NNE dip and is unconformably overlain by Natural Pasture basalt (Figure 3, 6 & 7). The Natural Pasture basalt is stratigraphically equivalent to the topographically flat Juniper Flats to the north, which extend northward from Mutton Mountain to Tygh Valley.

5.2 Mutton Mountain Structural Model

Mutton Mountain forms the core of a long-wavelength (15 km), northeast plunging antiform, which stands topographically high above the surrounding terrain. An Oligocene rhyolite dome complex forms the core of the anticline. The north limb of the anticline delineates the southern margin of Tygh Valley. Work by Smith (1986b) indicates a northeast trending syncline bounds the southern flank of Mutton

Mountain. The map pattern (Figure 2) of the Mutton Mountain rhyolite complex-CRBG contact defines the antiform and the structural lows to the south of Mutton Mountain, the Gateway syncline, and the Tygh Valley syncline to the north.

Mutton Mountain represented paleotopography at the time of the CRBG deposition, which limited their southern flow extent. CRBG flows lap on the north flank of the rhyolite complex and pinch-out below the crest of Mutton Mountain. Whereas onlap of the CRBG (~16 Ma) onto the northern flanks of the rhyolite dome complex explains thinning of CRBG flows to the south, it does not explain the 06° tilt to the north of the entire ~342 km² north flank of the mountain.

Surface unit exposures across Mutton Mountain decrease in age and degree of tilt from south to north, respectively. Mutton Mountain rhyolites dip 9°-15° to the northeast and are overlain by 06° north-northeast- dipping CRBG, which are overlain, in turn, by flat-lying Natural Pasture basalts to the north (Figures 3, 6 & 7). Pre-tilt slope of the Mutton Mountain rhyolite dome flanks would have been 3°-9° given the CRBG dip. On the basis of the interpretation that Mutton Mountain is cored by a rhyolite dome complex, the 3°-9° dip likely represents original dip of flows on dome flanks. These field relationships demonstrate that folding occurred between ~15.5 Ma and ~2.6 Ma, the ages of the CRBG and Natural Pasture basalts, respectively.

In spite of the fact that Mutton Mountain lies in close proximity (30 km) to the high Cascade graben fault and to Basin and Range faults to the south, an interpretation invoking normal faulting to explain tilt is inconsistent with the observation that large-scale folding dominates the surface structures (Figure 2). If extensional faults do

exist, they are limited to pre-Miocene units. Detailed mapping of the Oligocene and older rocks is required to test this hypothesis. Field data and map patterns therefore suggest that folding drove uplift of Mutton Mountain rather than footwall block rotation caused by extensional faulting.

5.3 Interpretation

Folding of the volcanic center began sometime during the Miocene and continued through the early Pliocene, tilting 28-29 Ma units of Mutton Mountain and 15.5 Ma CRBG, while late-Pliocene Natural Pasture basalt has been left relatively undeformed. Surface unit exposures across Mutton Mountain decrease in age and tilt from south to north. At the southern crest of Mutton Mountain are ~29 Ma rhyolites that dip 9°-15° to the northeast, overlain by ~15.5 Ma CRBG (Figures 3, 5 & 6). Flows of CRBG terminate against more steeply northeast dipping Mutton Mountain rhyolites and are uniformly tilted to the north-northeast at 06°. Pre-tilt slope of the Mutton Mountain rhyolite dome flanks would have to have been 3°-9° to result in post tilt dips of 9°-15°. Folding of Mutton Mountain must have commenced after 15.5 Ma as growth of the Mutton Mountain anticline tilted both the CRBG and its depositional contact with the rhyolites, 6° to the northeast. Flat lying Natural Pasture and Juniper Flats basalts constrain timing of folding here from post 15.5 Ma to mid-Pliocene as ~2.6 Ma basalt units remain relatively undeformed.

6. North flank: Tygh Valley to Tygh Ridge

Tygh Valley is a structural low separating the backlimb of the Mutton Mountain anticline and the southern flank of Tygh Ridge. Tygh Ridge is an

asymmetric anticline involving CRBG (Tgr) through late Pliocene lava flows (Tjfb, Thrb) (Figure 8). The Tygh Valley low rests between the steeply dipping forelimb of Tygh Ridge on the north and the shallowly-dipping, broad backlimb of Mutton Mountain anticline to the south. Dip changes systematically with age across the north side of the Tygh Valley low (Figure 8, B-B'). At Tygh Valley, mid-Pliocene volcanoclastic rocks (Ttv₂) and basalts (Thrb, Tjrb) are nearly flat lying. Outcrops of 8.4 Ma Ttv₁ dip steeply to the south-southeast and are in angular unconformity with the overlying 4.5 Ma Ttv₂ and 2.6 Ma Thrb (Figure 9A & B). An abrupt change in topography marks the transition from the south dipping limb of the Tygh Valley syncline to the forelimb of Tygh Ridge, which is held up by CRBG and rises ~518 m above younger flat lying basalts within the syncline (Figure 8 & 10).

6.1 Structural Relationships

Tygh Ridge can be broken into 3 segments along strike from east to west on the basis of structural changes along the fold axis. The eastern segment extends from the Deschutes River, 5 km to the west to point A on Figure 10. Although this segment was not mapped in detail, reconnaissance observations indicate a tight, asymmetric anticlinal fold where the backlimb dips gently to the north and the forelimb dips steeply to the south characterizes the fold geometry. Point A to point B at Butler

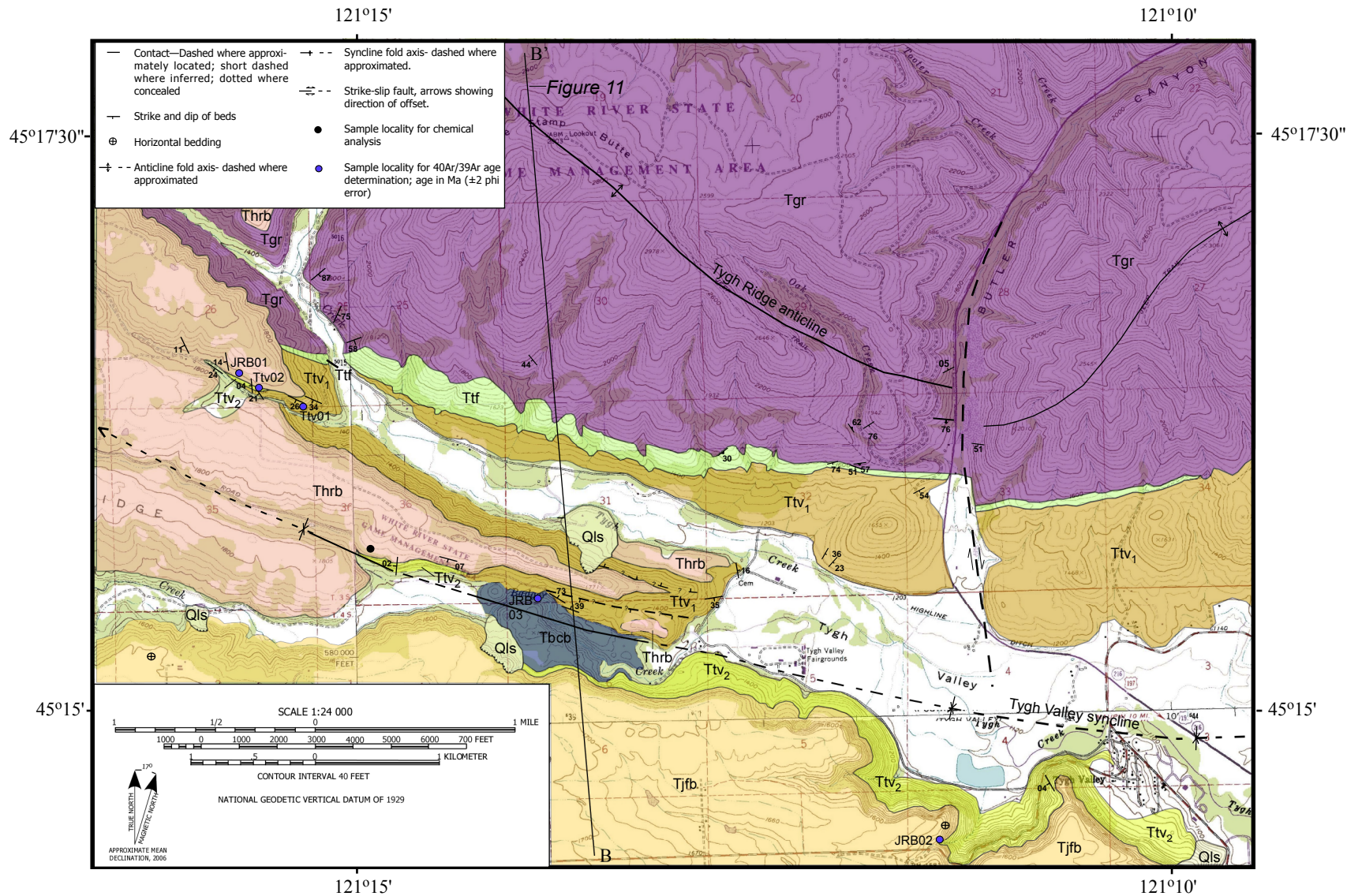


Figure 8. Geologic map of the south flank of Tygh Ridge. Blue dots denote $^{40}\text{Ar}/^{39}\text{Ar}$ sample names and localities. Refer to Plate 3 for larger version.

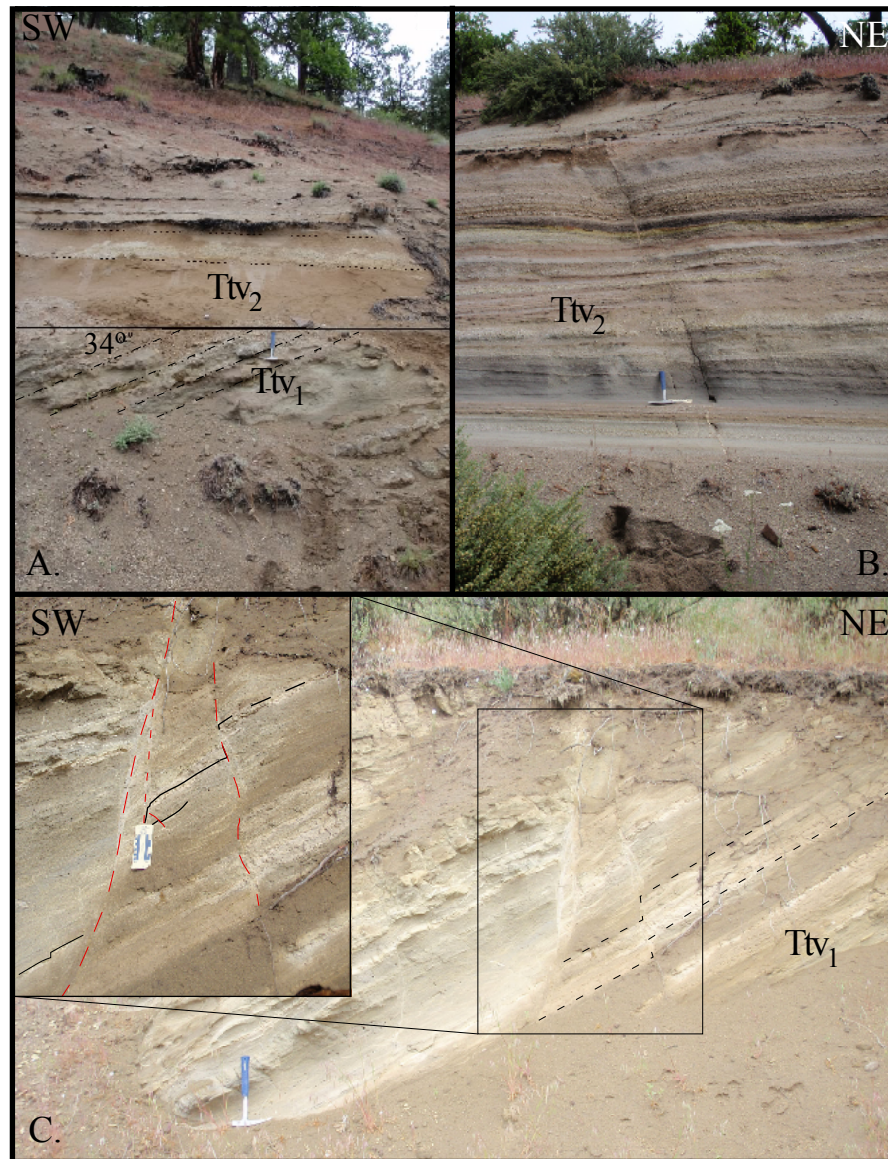


Figure 9. Outcrop features in the Tygh Valley volcaniclastic sequence. (A) Angular unconformity between Ttv₁ and Ttv₂. (B) Minimally tilted, reworked ash-flow tuffs of Ttv₂, showing minor displacement faulting. (C) Steep (70°-80°) NW striking faults with reverse separation in Ttv₁ evident less than 0.5 km from faults in B with similar trend.

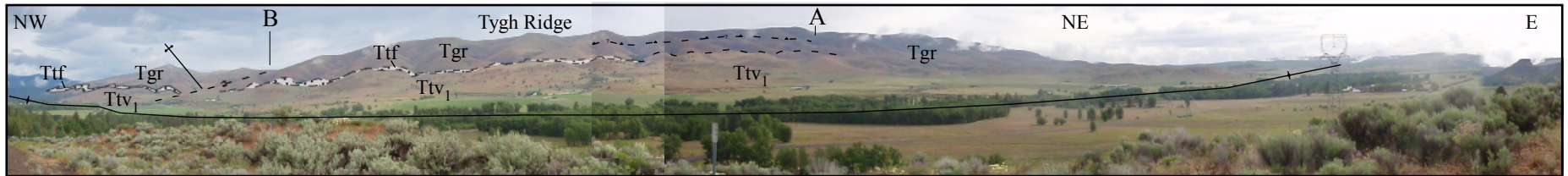


Figure 10. Northwest to northeast along strike panoramic view of Tygh Ridge from Tygh Valley (foreground). Ttf outcrops are marked by white stipple and dip 55° - 60° to the NNE. The Tygh Valley syncline runs through the low-relief valley bottom, marking where Tgr changes from steeply south dipping to gently north dipping. Points A and B are referenced in text.

Canyon (Figure 10) marks the second segment where the fold axial trace changes from an east-west orientation to a northwest-southeast trend (Figure 8). A north trending fault offsets the axial trace of the anticline at Butler Canyon (point B, figure 10) and forelimb dip increases from $\sim 30^\circ$ to nearly 80° to the west, marking the third segment of Tygh Ridge.

Along the forelimb of Tygh Ridge, Ttf conformably overlies CRBG and both dip steeply (51° - 74°) to the south-southeast. Near Butler Canyon CRBG strike and dip are $057/76^\circ$, respectively, and the basalt is conformably overlain by Ttf, which has a $070/74^\circ$ strike and dip. A 20° angular unconformity between 8.4 Ma Ttv₁ ($062/54^\circ$) and late Miocene Ttf, indicates folding of the forelimb of Tygh Ridge commenced sometime after 15 and before 8.4 Ma (Figure 9). A 30° angular unconformity separating Ttv₁ and Ttv₂ is revealed in a road cut west of Butler Canyon, indicating continued fold limb rotation between ~ 8.4 and ~ 4.5 Ma (Figure 9A).

Happy Ridge basalt to basaltic-andesite lava flows (2.59 ± 0.53 Ma) conformably overlie Ttv₂ (~ 4.5 Ma) at the western end of Tygh Valley. Juniper Flats basalt to the south is flat lying and onlaps Happy Ridge basalt indicating it is younger. At the forelimb of Tygh Ridge, Happy Ridge basalt has an attitude of $154/11^\circ$ and lies with angular unconformity over older units; Ttv₁, Ttf, and Tgr (Figure 9C). The volcanoclastic sediments (Ttv₁, Ttv₂) are only exposed at the western base of Tygh Ridge, where Tygh and Badger Creeks have eroded through the resistant lava flows.

An angular unconformity of $\sim 20^\circ$ formed between ~ 15 Ma CRBG and 8.4 Ma Ttv₁, a period of 6.1 Ma that indicates a tilting rate of $3.3^\circ/\text{Ma}$. An age of 3.9 Ma

between Ttv₁ and Ttv₂, which has an angular unconformity of 30°, gives a tilting rate of 7.7°/Ma. During the late Pliocene rate of tilting slowed. The ~2.6 Ma Happy Ridge basalt dips only shallowly to the south (11°) yielding a tilting rate of 4.4°/Ma from 2.5 Ma to the present. Change in tilting rate through the Pliocene could be attributed to a change in the rate of folding of the Tygh Ridge anticline, rate of change in limb rotation due to fold geometry, or both. Rotation of the forelimb of the Tygh Ridge anticline due to strike-slip shearing of the fold could also produce the change in tilting rate and angle of forelimb dip.

6.2 Faulting of Tygh Valley sediments

Small scale faults on the forelimb of Tygh Ridge cut the Ttv₁ and Ttv₂ sedimentary units, but do not have recognizable surface relief (Figure 8 & 9ABC). Northeast dipping faults (310/84°) in Ttv₁, appear to have greater separation than those found in the overlying, younger Ttv₂ (005/73°). In Figure 9C, steeply dipping fault strands (highlighted in red) suggest reverse or oblique motion but resolving this is difficult due to limited exposure of distinct marker bed offsets and slickenlines were not found. Reverse or oblique motion on a small set of northwest striking fault strands that dip to the northeast are consistent with southwestern limb rotation recorded by angular unconformities in Ttv₁ and Ttv₂ at the Tygh Ridge forelimb. The structural trend of the Tygh Ridge anticline is coincident with this trend of faulting, suggesting that these smaller strands may be related to a larger blind thrust at depth. Greater displacement of faults cutting Ttv₁ coincides with elevated rate of rotation recorded by

angular unconformities between 15.5 Ma Ttf/ 8.4 Ma, Ttv₁ and 8.4 Ma Ttv₁/ 4.5 Ma Ttv₂.

6.3 Tygh Valley structural model

Faults with orientations parallel to the trend of the Tygh Valley anticlinal axial trace cut the forelimb of Tygh Ridge. Steep dips attest to post CRBG growth of the Tygh Ridge anticline. Miocene CRBG through Pliocene Tygh Valley sediments (Ttf, Ttv₁ and Ttv₂) are exposed in the limb (Figure 10 & 11). Contact relationships constrain the temporal evolution of the anticline. A conformable contact marks the boundary between 15.5 Ma CRBG and Ttf, implying that folding initiated after Ttf deposition. Angular unconformities between Ttf and Ttv₁ and Ttv₁ and Ttv₂ indicate fold growth initiated sometime after ~15 Ma and continued until after 2.5 Ma.

It is unclear whether these faults are splays from a larger displacement fault at depth or represent localized shearing within the forelimb. It is interesting to note, however, that separation across the faults varies as a function of age. Similarly, the amount of bedding tilt, as documented by the angular unconformities, varies as a function of age as well. Greater separation across fault strands and steeper dips in Ttv₁ relative to the separation and tilt of the overlying Ttv₂ reveals that tilting rate during the early- to mid-Pliocene was higher than in the late Pliocene. North-south striking, right-lateral faults dominate faulting observable at map-scale. Tygh Ridge is

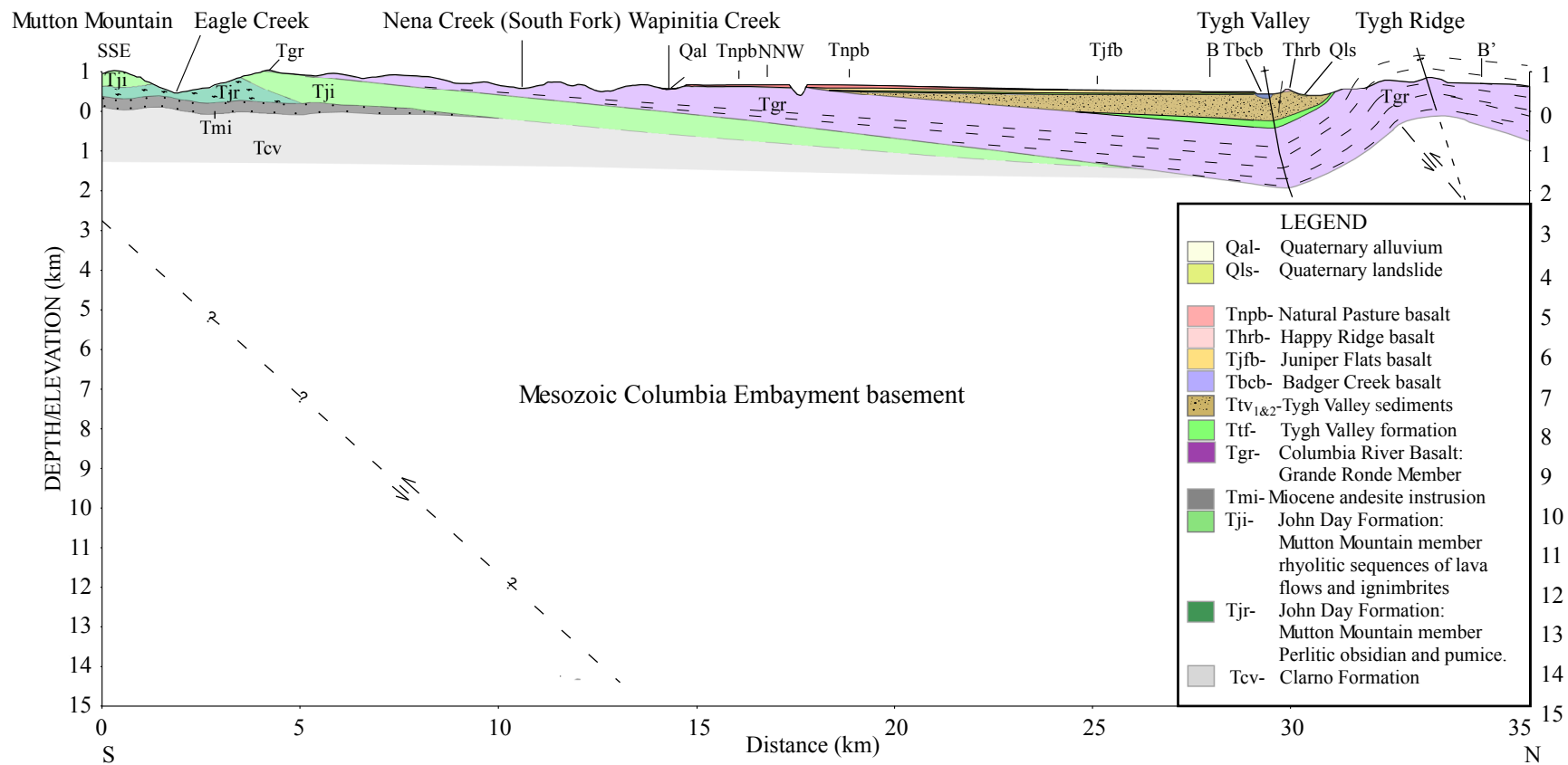


Figure 11. Composite cross-section from Mutton Mountain to Tygh Ridge across Tygh Valley. Cross-sections SSE-NNW and B-B' seen in Figures 3, 6 and 8 are noted, respectively. Dip and location of blind reverse faults at depth are depicted schematically. Refer to Plate 4 for larger version.

offset by such faults at several locations. The axial trace of Tygh Ridge is discontinuous, changing trend from nearly east-west in the east to northwest-southeast trending to the west of Butler Canyon, where it is offset by a north-trending fault (Figure 8). The difference in age and degree of dip between Ttv_1 and Ttv_2 reveals that tilting rate during the early- to mid-Pliocene was higher than in the late Pliocene.

North-south striking, right-lateral faults dominate faulting observable at map-scale. Tygh Ridge is offset such faults at several locations. The axial trace of Tygh Ridge is discontinuous, changing trend from nearly east-west in the east to northwest-southeast trending to the west of Butler Canyon, where it is offset by a north-trending fault (Figure 8).

Moment tensor solutions for local seismicity indicate that right-lateral strike-slip events with a strike of 355° , dominate active seismicity to the east of the Deschutes River, to the southeast of Tygh Ridge (Braunmiller and Trehu, 2008). Tygh Ridge is thus interpreted as a reverse fault-related fold segmented by, or forming in association with, north-striking faults with right-lateral separation.

7. Regional structural model

The regional model for the Tygh Valley field area includes two constraints. First are the geodetic constraints on dextral shear and north-south crustal shortening within the field area. Second are temporal constraints on shortening recorded by the geology.

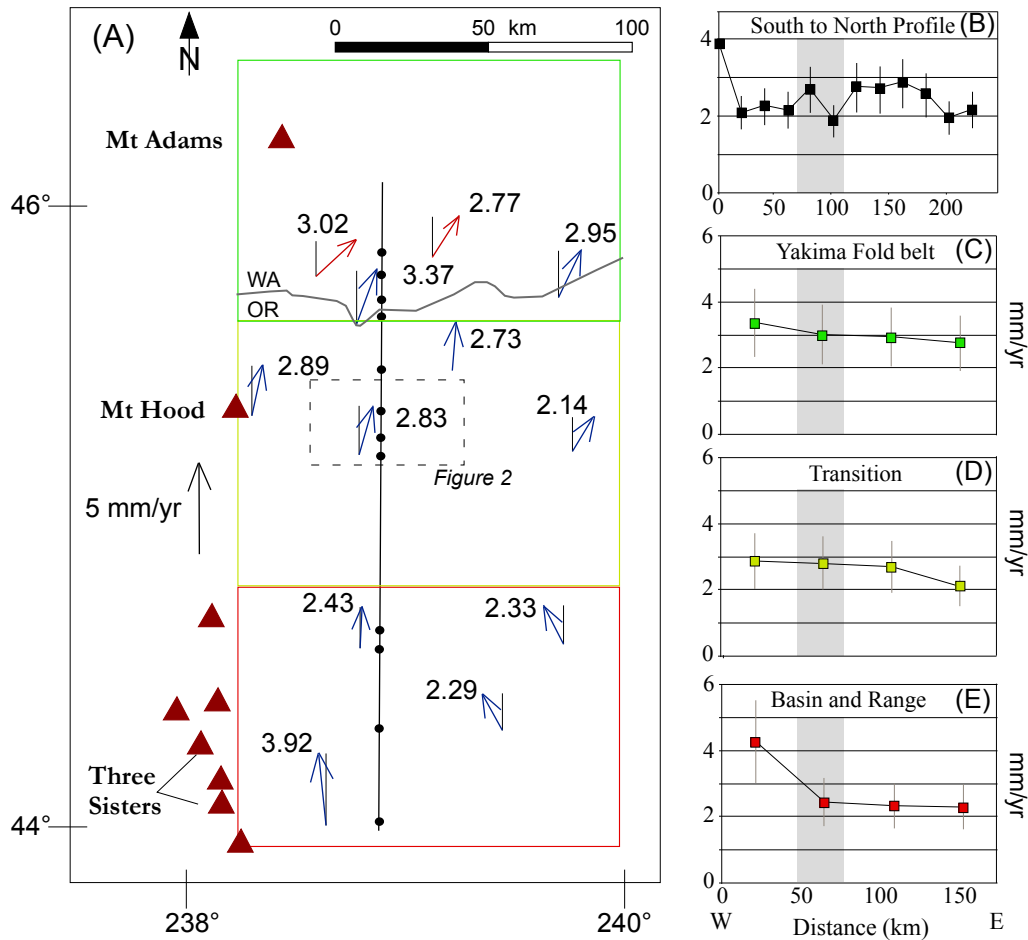


Figure 12. (A) Subset of geodetic data east of the Cascade arc. Vectors show velocity with respect to stable North America. (B) North component of each velocity vector from south to north (black line). Velocity field west to east for the Yakima fold belt (C), the transition region (D), and the Basin and Range (E). Grey bar indicates intersection of north-south profile in (A). GPS data from X, Y, Z.

7.1 Geodetic constraints on backarc deformation

Geodetic data reveal two distinct characteristics of deformation in the backarc (Figure 12). The vectors to the south in Figure 12 A, represent the northward extent of the Basin and Range Province and show the greatest northward velocities, ~ 3.9 mm/yr. North of the Basin and Range velocity region, velocities remain fairly consistent at ~ 2.3 - 2.8 mm/yr. Velocity data indicate that the northward component of motion (Figure 12 B) decreases northward across the transition region and YFB sections by ~ 1 mm/yr. This change in velocity provides geodetic evidence for the appearance of and continuation of crustal contraction and folding at the Mutton Mountain and Tygh Ridge anticlines.

A west to east decrease in velocity seen in Figure 12 C, D & E, indicates that distributed dextral shear occurs between the arc and the pole of rotation. This decrease from west to east, a distance defined by the boxed areas (Figure 12), implies right-lateral shear. Euler's Theorem would predict an increase in rotational velocity with distance relative to the "fixed" pole, eliminating the need for shear to accommodate for the west-east differential in velocity. However, the velocity gradient across the study area from the Cascade arc toward the pole is greater than that predicted by Euler's Theorem, necessitating dextral shear. Crustal shortening apparently occurs in the face of this dextral shear. Thus a model for transition region deformation must account for both the north-south shortening and the eastward diminishing dextral shear.

Dextral shear on geologic timescales is suggested by several field observations. Several dextral shears cut the Tygh Ridge anticline. Offset across Butler Canyon (Figures 8) and north striking strike-slip faults observed in CRBG east of the mapping area (Figure 10 A) are evidence of dextral shear. Both the Tygh Ridge and Mutton Mountain anticline axial traces trend progressively more northwesterly along strike from east to west, respectively (Figure 3 & 8). One interpretation is that dextral shear has rotated the fold axial traces from an east-west to a northwest-southeast orientation. Two scenarios relate dextral strike-slip faulting to the folds in the transition region (Figure 13). Folding in Tygh Ridge could reflect localized shortening associated with a left stepping compressional bend in through-going right-lateral strike-slip fault (Figure 13A). A through-going, strike-slip fault is not well supported by observations made in the field and the lack of large offsets that would reveal the location of a regionally continuous a strike-slip fault system.

An alternative model combines north-south contraction that drives the folding at Tygh Ridge and Mutton Mountain with distributed dextral shear. Dextral shear is manifested by north-trending right lateral faults that segment the fold axial trace and distributed shear that refolds the axial trace (Figure 13 B). Moment tensor solutions from earthquakes to the east of the Deschutes River indicate right-lateral strike-slip motion on north-northwest trending planes (Figure 2). In this model, extension in the Cascade arc across the Hood River normal fault occurs independently of deformation in the Tygh Valley region to the east (Figure 13B).

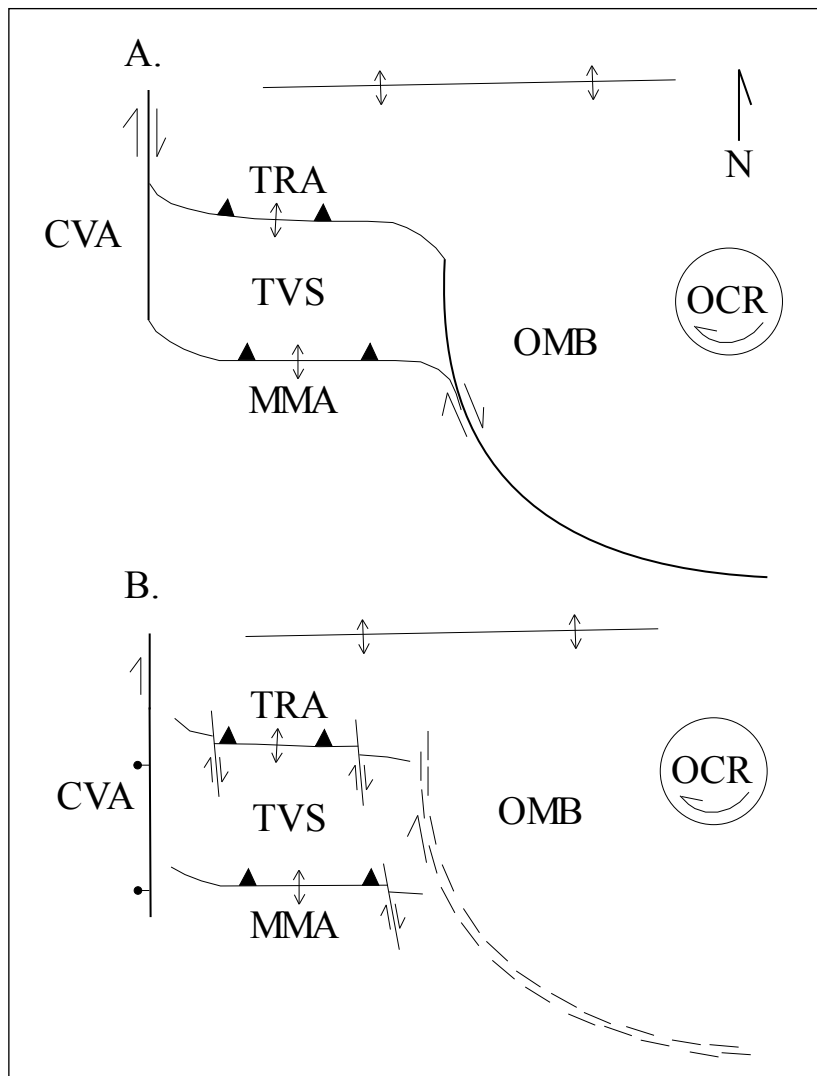


Figure 13. End member models of the transition region. A. Folding at Tygh Valley is attributed to a contractional bend in a larger strike-slip fault system. B. Folding at Tygh Valley is attributed to the transition from extension (south) to contraction (north), is bound by a dextral distributed shear zone to the east and Cascade graben faults to the west. CVA: Cascade Volcanic arc, TRA: Tygh Ridge anticline, TVS: Tygh Valley syncline, MMA: Mutton Mountain anticline, OMB: Ochoco Mountain block, OCR: Oregon Coast Range block (McCaffrey, et. al., 2007; Wells, 1998).

7.2 Rate and Time Scale of Shortening

Timing of folding in Tygh Valley is constrained by the structural relationships of Oligocene to Pliocene exposures in the region. To the south in Mutton Mountain, an angular unconformity between ~29.5 Ma rhyolites and 15.5 Ma CRBG is exposed.

A 3°-6° angular unconformity between the youngest Oligocene rhyolites and the CRBG is explained by onlap of basalt flow against the paleo-slope of the rhyolite dome complex. Few constraints on folding exist prior to 15.5 Ma as Oligocene units within Mutton Mountain are <1 m.y. of one another and are relatively conformable.

Overlying CRBG, south of Tygh Valley and north of Mutton Mountain are ~2.6 Ma, flat lying basalts of Natural Pasture and Juniper Flats. A 3°-6° angular unconformity between CRBG and the Natural Pasture basalt is due to the 6° tilt of the CRBG prior to deposition of the younger basalt. Relationships between these units indicate that tilting of the Mutton Mountain backlimb since 2.6 Ma has not been substantial enough to tilt the youngest basalt flows.

Contact relationships between Pliocene units in the forelimb of Tygh Ridge anticline constrain the onset and rate of rotation here. Conformably overlying CRBG at the northern boundary of Tygh Valley is the late-Miocene Ttf. An angular unconformity of ~30° separates mid-Pliocene Ttv₂ from Late Miocene Ttv₁ which constrains the onset of folding to the late Miocene (between 15 and 9 Ma). Faulting of both the 8.4 Ma Ttv₁, the 4.5 Ma Ttv₂ and tilt of the Happy Ridge basalt suggests that folding continued through the Pliocene and after 2.6 Ma. Greater displacement along

fault strands and steeper dips in Ttv₁ than Ttv₂ indicate limb rotation was consistent through the early-to mid-Pliocene. Late-Pliocene basaltic-andesite lava flows in conformable contact with Ttv₂, are near flat-lying within Tygh Valley and dip 11° to the south at the Tygh Ridge forelimb. The 2.6 Ma Happy Ridge flow overlies the contact between the CRBG and all Pliocene units. As it approaches the forelimb of Tygh Ridge, the change in dip of the Happy Ridge basalt (from 0° to 11°) is testament to continued rotation of the Tygh Ridge forelimb in the last 2.6 Ma.

Folding of the Tygh Ridge anticline during the mid- to late-Pliocene forced basalt flow deposition successively to the south, away from the forelimb. Younger and less deformed flows appear to the south of older flows. If rotation rate on the backlimb of Mutton Mountain is slower than that of the forelimb of Tygh Ridge, the lack of tilt between CRBG and the Natural Pasture basalt may reflect the low backlimb rotation rate.

Calculating shortening using the cross-section allows for minimum estimates of shortening over a timescale of 10⁶ Ma (Figure 11). Calculation of crustal shortening across the Mutton Mountain and Tygh Ridge anticlines is challenging because few correlative units are found in both folds. By projecting the CRBG from the crest of the Mutton Mountain anticline into the subsurface of the Tygh Valley syncline, minimum shortening for the backlimb of Mutton Mountain anticline is estimated to be 0.8 km or 3% ($\pm 0.3\%$) for a shortening rate of 0.6 mm/yr from 15.5 to 2.6 Ma. Since only the backlimb of the Mutton Mountain anticline is included in this approximation, this north-south shortening is a conservative minimum. Maximum

shortening rate of the backlimb is estimated at ~ 0.14 mm/yr for the period between 8.4 and 2.6 Ma.

By measuring the deformed length of a projected Ttf unit in cross-section and calculating undeformed length from B-B' (Figure 11), a minimum total shortening across Tygh Ridge is estimated. Crustal shortening is approximated to be 0.58 km or 8.4% ($\pm 0.8\%$) across the Tygh Ridge forelimb (from B-B' on Figure 11), for a minimum rate of 0.05 mm/yr from 15.0 to 2.6 Ma. Maximum shortening rate between 8.4 and 2.6 Ma is estimated at ~ 0.13 mm/yr. No oblique or strike-slip motion is accounted for in this estimate and therefore actual rate of deformation may be larger.

An average of 5.5% ($\pm 0.5\%$) shortening is calculated from the Tygh Ridge anticline crest to the Mutton Mountain anticline crest, a fold wavelength of ~ 15 km (Figure 11). A $\sim 5\%$ shortening rate is consistent with average shortening across the Yakima fold belt (Reidel et al. 1989). Based on data collected during this study, the most active period for folding in the transition region was through the mid-Pliocene (8.4 Ma- 4.5 Ma) when as much as 50% of the tilting is recorded.

8. Implications for transition region

Whereas a transition region between crustal extension to the south in the Basin and Range and contraction in the Yakima fold belt to the north is required, the Mutton Mountain to Tygh Ridge fold train must lie to the north of the zone of transition. Tygh Ridge and Mutton Mountain, the structures bounding Tygh Valley are interpreted as the southwestern thrust front of the Yakima fold belt. Crustal

shortening created long wavelength, asymmetrical, anticlinal ridges that extend eastward from the high Cascades where it appears that the axial trace is truncated by the north-trending Hood River valley normal fault (Figure 13 B). The long wavelength, asymmetric anticlines separated by synclinal valleys structural style of Tygh Ridge, south to Mutton Mountain bears close similarity to that of the Yakima folds (Reidel, 1984).

Where is the transition region? A narrow (<35 km) transition region marks the change from extension to contraction within the backarc. The transition region is something of a misnomer, because existing data do not indicate a zone of mixed mode normal and reverse faulting. Rather the 'transition region' is in fact a relatively narrow undeformed block separating the Gateway syncline (Smith, 1986) from the northern-most extensional faults. The transition region is bound to the west by the Cascade arc graben and to the east by a shear zone separating it from the relatively stable Ochoco Mountain block (OMB) (Figure 13).

8.1 A structural model for backarc accommodation of clockwise rotation

Right-lateral, north-south striking transform shears are common features in the southern Yakima fold belt (Reidel et al., 2003; Wells and Heller, 1988). Orientation of fold axes changes from south to north across the Yakima fold belt. Axial trace strike of Yakima folds change by 15°-20° from an east-west to a northwest-southeast trend. In the Yakima fold belt, Wells (1998) identified dextral shear through paleomagnetic data of the CRBG, indicating backarc rotation.

Dextral shear of the Tygh Ridge anticline can be inferred from offset of the Tygh Ridge axial trace and rotation of the Mutton Mountain anticline axial trace (Figure 13). Offset across Butler Canyon and north trending strike-slip faults observed in CRBG east of the mapping area, in Figure 8, support a component of dextral shear accompanying folding. Change in orientation of the axial trace implies rotation of Tygh Ridge anticline, from an east-west orientation (found east of the mapped area in Figure 8) to northwest trend ($\sim 290^\circ$) west of Butler Canyon (Figure 13). A similar style of axial rotation is observed along the Mutton Mountain anticline where the axial trace changes trend from nearly east-west orientation to northwest at its western end (Figure 13). Change in strike of the axial traces and dextral offsets reflect a broad shear zone which transfers motion between the relatively stable OMB to the northward moving Cascade arc.

The BFZ is a northwest-southeast striking zone of relatively small normal faults, oblique to much larger Basin and Range faulting to the south (Meigs et al., 2009; Trench, 2008a). The BFZ separates the stable OMB from the Basin and Range extensional province to the south. Motion across the fault zone is dominated by northeast-directed extensional motion, with a moderate to small component of right-lateral strike slip displacement (Figure 14) (Lawrence, 1978; McCaffrey et al., 2007; Meigs et al., 2009; Trench, 2008a).

The graben system bounding the stratovolcanoes of the present Cascade arc marks the western boundary of the back arc structural province. North-trending normal faults down-dropped the Cascade graben system from southern Oregon to southern

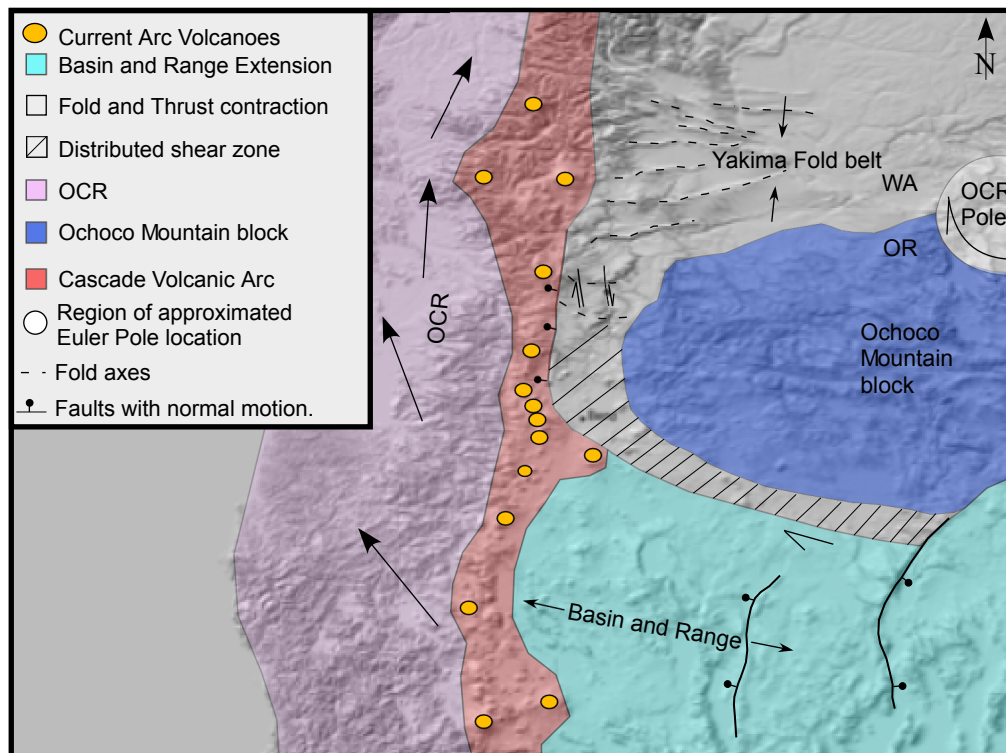


Figure 14. Regional tectonic model for backarc deformation in the Pacific Northwest. Rotation of the OCR (pink) drives crustal extension in the Basin and Range (green), contraction in the Yakima Fold (dashed lines represent fold axes), and requires that the transition region include shortening and dextral shear (hash marks) (see Figure 11, 12 & 13). The Ochoce Mountain block (OBM, blue) represents a relatively stable block with little internal deformation. Grey circle marks range of proposed OCR rotational pole locations (Hammond and Thatcher, 2005; McCaffrey et al., McCaffrey et al., 2007; Wells et al., 1998).

Washington (Conrey, 1985). Arc-parallel normal faulting to the west of Tygh Valley likely accommodates the velocity gradient between the arc and pole of rotation.

8.2 Mutton Mountain and regional Oligocene volcanism

Orientation of Oligocene rhyolite volcanic centers apparently reflects clockwise rotation in the back arc as well (Wells, 2009). The Mutton Mountain rhyolite dome complex, 28.56 ± 0.15 to 29.14 ± 1.09 Ma, is of the same age as a number of other rhyolite centers across southeastern Oregon; Gray Butte (28.8 ± 0.23 Ma) (Smith, 1986b), Hampton Butte (30.39 ± 0.25 Ma) (Iademarco, 2009) and Crooked River Caldera (McClaughry et al., 2009). It is feasible that these volcanic centers represent the easternmost Oligocene location of a broad paleo-Cascade arc, recording rotation rate and direction of arc migration since that time.

The Mutton Mountain volcanic center formed temporally with Member G of the John Day Formation and the rhyolites of Gray Butte (Christiansen et al., 1992; McClaughry et al., 2009; Robinson, 1973; Smith et al., 1987; Taylor, 1973). Rhyolite lava flows from the Mutton Mountain rhyolite complex are thick and chemically similar to the local rhyolitic dike (Tjd) suggesting this may be a source for these flows.

Observations including age and geochemical correlations between rhyolites from Mutton Mountain and those from Gray Buttes (which were correlated by Smith to Member G of the John Day Formation) indicate the Mutton Mountain volcanic center could have sourced at least a portion of the rhyolitic material found at Gray Buttes (Table 3) (McClaughry et al., 2009; Robinson, 1973; Smith et al., 1987).

9. Conclusions

The transition between crustal extension in southeastern Oregon and contraction in north-central Oregon is defined in the backarc by a discrete region where rotational and northward motion associated with the forearc block decreases. A velocity gradient decline from west to east indicated by GPS data combined with geologic timescale structural data places this region approximately between Bend, Maupin, the Cascade arc, and the Ochoco Mountains.

The evolution of geologic units and structural features found within Tygh Valley and Mutton Mountain since the Oligocene are as follows:

During the Oligocene (28.5 to ~30 Ma) extensive rhyolitic volcanism generated a thick sequence of silicic rhyolite domes centered at Mutton Mountain. Geochemically and temporally, these rhyolites correlate with the Gray Buttes rhyolites. By the early Miocene, rhyolitic volcanism ended and by ~16 Ma CRBG flows began lapping onto the flanks of the rhyolite dome complex, burying both topography and earlier sedimentary deposits. Flows of the CRBG continued through the mid Miocene, thickening to ~1 km north of the Mutton Mountain rhyolite complex. During the late Miocene, volcanic eruptions, possibly sourced from the proto-high Cascades deposited volcanoclastic sediments conformably on the CRBG.

In the late Miocene, folding of the region commenced, tilting the Tygh Ridge forelimb of CRBG and its conformable contact with Ttv₁. During the early- to mid-Pliocene, folding occurred in both the Mutton Mountain and Tygh Ridge anticlines.

Folding through the early- to mid-Pliocene is recorded by $<30^\circ$ angular unconformities between sedimentary packages deposited in the Tygh Valley synclinal basin. Late-Pliocene basaltic-andesite flows with shallow dips attest to slow, but continuous limb rotation that persisted after 2.6 Ma. The most active period for folding in the transition region was through the mid-Pliocene (8.4 Ma- 4.5 Ma) when as much as 50% of the tilting is recorded. Post-Pliocene folding is masked by detritus supplied from the growing Cascade arc.

Tygh Valley is bound to the west by the Cascade arc graben and to the east by a diffuse shear zone separating it from the relatively stable Ochoco Mountain Block (OMB). Change in strike of the axial traces and dextral offsets reflect a broad shear zone which transfers motion between the relatively stable OMB to the northward moving Cascade arc. Arc-parallel normal faulting to the west of Tygh Valley likely accommodates the velocity gradient between the arc and pole of rotation. Transition between backarc extension and contraction in response to arc and forearc motion about a rotational pole occurs in a relatively small region where dextral shear and crustal shortening occur in concert to accommodate for larger scale deformation.

Further work in north-central Oregon and the transition region is required to resolve geological issues and to place better estimates on the timing of events here. Petrologic study of the Deschutes and Tygh Valley formations and the rhyolite complex of Mutton Mountain would lead to a greater understanding to the evolution of magma generation. In order to better resolve fault plane location and depth sourcing of current seismic activity, a local magnetic or gravity survey would be beneficial.

The tectonic and structural evolution of the transition region is a key piece in the geologic story of the Cascade backarc. Having a better understanding of each geologic aspect will help define what role the transition region plays in the larger tectonic picture of the Pacific Northwest.

References

- Bela, J., 1982, Geologic compilation map of The Dalles 1 x 2 degree quadrangle, Oregon and Washington: State of Oregon Department of Geology and Mineral Industries, p. 2.
- Braunmiller, J., and Trehu, A., 2008, The Maupin, Oregon Earthquake swarm: unpublished, p. 5.
- Campbell, N., and Bentley, R.D., 1981, Late Quaternary deformation of the Toppenish Ridge uplift in south-central Washington: *Geology*, v. 9, p. 519-524.
- Christiansen, R.L., Yeats, R.S., Graham, S.A., Niem, A.R., Niem, W.A., and Snavely, P.D., 1992, Post-Laramide geology of the U.S. Cordilleran region, The Cordilleran Orogen: Cotermminus U.S., Volume G-3 The Geology of North America: Boulder, CO, Geological Society of America, p. 261-406.
- Conrey, R.M., 1985, Volcanic stratigraphy of the Deschutes Formation, Green Ridge to Fly Creek, north-central Oregon: Master's thesis, v. Oregon State University, p. 365.
- Farooqui, S.M., Beaulieu, J.D., Bunker, R.C., Stensland, D.E., and Thoms, R.E., 1981, Dalles Group: Neogene formations overlying the Columbia River Basalt Group in north-central Oregon: *Oregon Geology*, v. 43, p. 16.
- Gordon, R.G., 1998, The Plate Tectonic Approximation: Plate Nonrigidity, Diffuse Plat Boundaries, and Global Plate Reconstructions: *Annu. Rev. Earth Planet. Sci.*, v. 26, p. 27.

- Hammond, W.C., and Thatcher, W., 2005a, Northwest Basin and Range tectonic deformation observed with the Global Positioning System, 1999-2003: *Journal of Geophysical Research*, v. 110, p. 12.
- , 2005b, Northwest Basin and Range tectonic deformation observed with the Global Positioning System, 1999–2003: *Journal of Geophysical Research*, v. 110, p. 12.
- Heller, P.L., Tabor, R.W., and Suczek, C.A., 1987, Paleogeographic evolution of the United States Pacific Northwest during Paleogene time: *Canadian Journal of Earth Science*, v. 24, p. 16.
- Heuret, A., and Lallemand, S., 2004, Plate motions, slab dynamics and back-arc deformation: *Physics of the Earth and Planetary Interiors*, v. 149, p. 20.
- Hooper, P.R., Conrey, R.M., Smith, G.A., Anderson, J.L., Bailey, D.G., Beeson, M.H., Tola, T.L., and Urbanczyk, K.M., 1993, The Prineville basalt, north-central Oregon: *Oregon Geology*, v. 55, p. 24.
- Iademarco, M.J., 2009, Volcanism and faulting along the Northern margin of Oregon's High Lava Plains: Hampton Butte to Dry Mountain: Master's thesis, p. 158.
- Johnson, D.M., Hooper, P.R., and Conrey, R.M., 1999, XRF Analysis of Rocks and minerals for Major and trace Elements on a Single Low Dilution Li-tetraborate Fused Bead: *Advances in X-ray Analysis*, v. 41, p. 23.
- Kreemer, C., and Hammond, W.C., 2007, Geodetic constraints on areal changes in the Pacific-North America plate boundary zone: What controls Basin and Range extension: *Geology*, v. 35, p. 5.

- Lawrence, R.D., 1976, Strike-slip faulting terminates the Basin and Range province in Oregon: Geological Society of America Bulletin, v. 87, p. 846-850.
- , 1978, Strike-slip faulting terminates the Basin and Range province in Oregon: Geological Society of America Bulletin, v. 87, p. 5.
- Magill, J.R., Wells, R.E., Simpson, R.W., and Cox, A.V., 1982, Post 12 m.y. Rotation of Southwest Washington: Journal of Geophysical Research, v. 87, p. 16.
- Mangan, M.T., Wright, T.L., Swanson, D., A., and Byerly, G.R., 1986, Regional correlation of Grande Ronde Basalt flows, Columbia River Basalt Group, Washington, Oregon, and Idaho: Geological Society of America Bulletin, v. 97, p. 20.
- Mann, G.M., and Meyer, C.E., 1993, Late Cenozoic structure and correlations to seismicity along the Olympic-Wallowa lineament, northwest United States: Geological Society of America Bulletin, v. 105, p. 853-871.
- McCaffery, R., Qamar, A.I., King, R.W., Wells, R., Khazaradze, G., Williams, C., Stevens, C.W., Vollick, J.J., and Zwick, P.C., 2007, Fault locking, block rotation and crustal deformation in the Pacific Northwest: Geophysical Journal International, v. 169, p. 1315-1340.
- McCaffrey, R., Long, M.D., Goldfinger, C., Zwick, P.C., Nabalek, J.L., Johnson, C.K., and Smith, C., 2000a, Rotation and plate locking at the southern Cascadia subduction zone: Geophysical Research Letters, v. 27, p. 4.

- McCaffrey, R., Long, M.D., Goldfinger, C., Zwick, P.C., Nabelek, J.L., Johnson, C.K., and Smith, C., 2000b, Rotation and plate locking at the southern Cascadia subduction zone: *Geophysical Research Letters*, v. 27, p. 3117-3120.
- McCaffrey, R., Qamar, A.I., King, R.W., Wells, R.E., Khazaradze, G., Williams, C.A., Stevens, C.W., Vollick, J.J., and Zwick, P.C., 2007, Fault locking, block rotation and crustal deformation in the Pacific Northwest: *GJI Tectonics and geodynamics*, v. 169, p. 27.
- McCloughry, J.D., Ferns, M.L., and Gordon, C.L., 2009, Field trip guide to the Neogene stratigraphy of the Lower Crooked Basin and the ancestral Crooked River, Crook County, Oregon: *Oregon Geology*, v. 69, p. 16.
- McCloughry, J.D., Ferns, M.L., Gordon, C.L., and Patridge, K.A., 2009, Field trip Guide to the Oligocene Crooked River caldera: Central Oregon's Supervolcano, Crook, Deschutes, and Jefferson Counties, Oregon.: *Oregon Geology*, v. 69, p. 19.
- Meigs, A.J., Scarberry, K.C., Grunder, A.L., Carlson, R., Ford, M.T., Fouch, M., Grove, T., Hart, W.k., Iademarco, M.J., Jordan, B.T., Milliard, J.B., Streck, M.J., Trench, D., and Weldon, R., 2009, Geological and geophysical perspectives on the magmatic and tectonic development, High Lava Plains and northwest Basin and Range: *Geological Society of America Field Guide*, v. 15, p. 36.

- O'Connor, J.E., Curran, J.H., Beebee, R.A., Grant, G.E., and Sarna-Wojcicki, A., 2002, Quaternary Geology and Geomorphology of the Lower Deschutes River Canyon, Oregon: AGU Water Science and Application, v. 7, p. 22.
- Pezzopane, S.K., and Weldon, R.J., 1993a, Tectonic Role of Active Faulting in Central Oregon: Tectonics, v. 12, p. 30.
- Pezzopane, S.K., and Weldon, R.J.I., 1993b, Tectonic role of active faulting in central Oregon: Tectonics, v. 12, p. 1140-1169.
- Reidel, S.P., 1983, Stratigraphy and petrogenesis of the Grand Ronde Basalt from the deep canyon country of Washington, Oregon and Idaho: Geological Society of America Bulletin, v. 94, p. 25.
- , 1984, The Saddle Mountains: the evolution of an anticline in the Yakima fold belt: American Journal of Science, v. 284, p. 37.
- Reidel, S.P., Fecht, K.R., Hagood, M.C., and Tolan, T.L., 1989a, The geologic evolution of the central Columbia Plateau, *in* Reidel, S.P., and Hooper, P.R., eds., Volcanism and tectonism in the Columbia River flood-basalt province, Volume Special Paper 239: Boulder, Geological Society of America, p. 247-264.
- Reidel, S.P., Martin, B.S., and Petcovic, H.L., 2003, The Columbia River flood basalts and the Yakima fold belt: Geological Society of America Field Guide, v. 4, p. 20.
- Reidel, S.P., Tolan, T.L., Hooper, P.R., Beeson, M.H., Fecht, K.R., Bentley, R.D., and Anderson, J.L., 1989b, The Grande Ronde Basalt, Columbia River Basalt

Group; Stratigraphic descriptions and correlations in Washington, Oregon, and Idaho, *in* Reidel, S.P., and Hooper, P.R., eds., *Volcanism and Tectonism in the Columbia River Flood-Basalt Province*, Volume Special Paper 239: Boulder, Colorado, Geological Society of America, p. 32.

Robinson, P.T., 1973, John Day Formation and Columbia River Basalt. Field Trips in northern Oregon and Southern Washington; The Cretaceous and Cenozoic, north-Central Oregon: Bulletin- State of Oregon Department of Geology and Mineral Industries, v. 77, p. 4.

Scarberry, K.C., Meigs, A.J., and Grunder, A.L., 2009, Faulting in a Propagating continental rift: Insight from the Late Miocene structural development of the Abert Rim fault, Southern Oregon, USA: *Tectonophysics*, v. 488, p. 15.

Smith, G.A., 1986a, Simtustus Formation: Paleogeographic and stratigraphic significance of a newly defined Miocene unit in the Deschutes basin, central Oregon: *Oregon Geology*, v. 48, p. 16.

—, 1986b, The Influence of Explosive Volcanism on fluvial sedimentation: The Deschutes Formation (Neogene) in Central Oregon: *Journal of Sedimentary Petrology*, v. 57, p. 17.

Smith, G.A., Manchester, S.R., Ashwill, M., McIntosh, W.C., and Conrey, R.M., 1998, Late Eocene-early Oligocene tectonism, volcanism, and floristic change near Gray Butte, central Oregon: *Geological Society of America Bulletin*, v. 110, p. 20.

- Smith, G.A., Snee, L.W., and Taylor, E.M., 1987, Stratigraphic, sedimentologic, and petrologic record of the late Miocene subsidence of the central Oregon High Cascades: *Geology*, v. 15, p. 4.
- Taylor, E.M., 1973, Geology of the Deschutes Basin. Geologic Field Trips in Northern Oregon and Southern Washington; Trip 1, Cretaceous and Cenozoic, North-Central Oregon. : Bulletin- State of Oregon Department of Geology and Mineral Industries, v. 77.
- Tolan, T.L., Reidel, S.P., Beeson, M.H., Anderson, J.L., Fecht, K.R., and Swanson, D., A., 1989, Revisions to the estimates of the areal extent and volume of the Columbia River Basalt Group, *in* Reidel, S.P., and Hooper, P.R., eds., *Volcanism and Tectonism in the Columbia River Flood-Basalt Province*, Volume Special Paper 239: Boulder, Colorado, Geological Society of America, p. 20.
- Trench, D., 2008a, The Termination of the Basin and Range Province into a Clockwise Rotating Region of Transtension and Volcanism, Central Oregon: Master's thesis, v. Oregon State University, p. 64.
- Uppuluri, V.R., 1974, Prineville Chemical Type: A New Basalt Type in the Columbia River Group: *Geological Society of America Bulletin*, v. 85, p. 5.
- Wells, e.a., 1998, Fore-arc migration in Cascadia and its neotectonic significance: *Geology*, v. 26, p. 759-762.

- Wells, R.E., 1990 Paleomagnetic Rotations and the Cenozoic Tectonics of the Cascade Arc, Washington, Oregon, and California: *Journal of Geophysical Research*, v. 95, p. 9.
- , 2009, Neogene magmatism and block motions in the Pacific Northwest: *Geological Society of America Abstracts with Programs*, v. 41, p. 1.
- Wells, R.E., and Heller, P.L., 1988, The relative contribution of accretion, shear, and extension to Cenozoic tectonic rotation in the Pacific Northwest: *Geological Society of America Bulletin*, v. 100, p. 15.
- Wells, R.E., Weaver, C.S., and Blakely, R.J., 1998, Fore arc migration in Cascadia and its neotectonic significance: *Geology*, v. 26, p. 759-762.
- West, M.W., Ashland, F.X., Busacca, A.J., Berger, G.W., and Shaffer, M.E., 1996, Late Quaternary deformation, Saddle Mountains anticline, south-central Washington: *Geology*, v. 24, p. 1123-1126.
- Zoback, M.L., Anderson, R.E., and Thompson, G.A., 1981, Cenozoic evolution of the state of stress and style of tectonism of the Basin and Range province of the western United States: *Philosophical Transactions of the Royal Society of London*, v. A-300, p. 27.

Incremental Heating									
	36Ar(a)	37Ar(ca)	38Ar(cl)	39Ar(k)	40Ar(r)	Age ± 2σ (Ma)	40Ar(r) (%)	39Ar(k) (%)	K/Ca ± 2σ
10C3301	500 °C	0.028287	0.036169	0.000138	0.004428	46.83 ± 24.63	0.079611	12.47	0.053 ± 0.002
10C3302	600 °C	0.003305	0.123517	0.000020	0.003985	2.99 ± 3.59	0.004522	11.23	0.014 ± 0.000
10C3303	700 °C	0.000898	0.186949	0.000004	0.004943	2.79 ± 1.48	0.005224	13.93	0.011 ± 0.000
10C3304	800 °C	0.000498	0.253074	0.000013	0.006079	2.56 ± 0.79	0.005894	17.12	0.010 ± 0.000
10C3306	900 °C	0.000258	0.190170	0.000012	0.004359	2.56 ± 1.35	0.004228	12.28	0.010 ± 0.000
10C3307	1000 °C	0.000347	0.156479	0.000016	0.003307	2.48 ± 1.71	0.003109	9.32	0.009 ± 0.000
10C3308	1100 °C	0.000327	0.115621	0.000031	0.002382	2.46 ± 1.88	0.002222	6.71	0.009 ± 0.000
10C3309	1200 °C	0.000693	0.118791	0.000029	0.002308	3.18 ± 9.98	0.002783	6.50	0.008 ± 0.000
10C3311	1300 °C	0.000538	0.112932	0.000028	0.001980	2.61 ± 2.53	0.001958	5.58	0.008 ± 0.000
10C3312	1400 °C	0.000878	0.097941	0.000027	0.001728	2.86 ± 5.09	0.001878	4.87	0.008 ± 0.000
Information on Analysis									
Results									
JRB 01	Weighted Plateau		40(r)/39(k) ± 2σ		Age ± 2σ (Ma)		Σ 39Ar(k) (%)		K/Ca ± 2σ
groundmass	0.9816 ± 0.2017 ± 20.55%		0.02		2.59 ± 0.53 ± 20.56%		87.53		0.009 ± 0.001
Or	External Error ± 0.53		2.31		Statistical T Ratio		9		
jh	Analytical Error ± 0.53		1.0000		Error Magnification				
Project = HLP	Total Fusion Age		3.1389 ± 1.2395 ± 39.49%		8.26 ± 3.26 ± 39.41%		10		0.011 ± 0.000
Irradiation = OSU3B10	J = 0.0014627 ± 0.0000076		External Error ± 3.26		Analytical Error ± 3.26				
FCT-3 = 28.030 ± 0.003 Ma									

Incremental Heating		36Ar(a)	37Ar(ca)	38Ar(cl)	39Ar(k)	40Ar(r)	Age ± 2σ (Ma)	40Ar(r) (%)	39Ar(k) (%)	K/Ca ± 2σ
10C1407	400 °C	0.002134	0.001370	0.000065	0.003241	0.051189	47.03 ± 7.32	7.51	0.72	1.017 ± 0.103
10C1408	500 °C	0.002473	0.005621	0.000099	0.014503	0.105896	21.90 ± 2.15	12.66	3.20	1.109 ± 0.056
10C1410	600 °C	0.003394	0.021173	0.000271	0.051092	0.316565	18.60 ± 0.59	23.99	11.29	1.038 ± 0.050
10C1411	700 °C	0.001421	0.026612	0.000269	0.049149	0.276425	16.89 ± 0.50	39.69	10.86	0.794 ± 0.040
10C1412	775 °C	0.001530	0.045257	0.000377	0.065408	0.343370	15.77 ± 0.48	43.17	14.45	0.621 ± 0.030
10C1413	825 °C	0.001041	0.040925	0.000285	0.048986	0.255531	15.67 ± 0.41	45.38	10.82	0.515 ± 0.025
10C1415	900 °C	0.000964	0.046738	0.000286	0.045073	0.235307	15.68 ± 0.52	45.24	9.96	0.415 ± 0.020
10C1416	1000 °C	0.001601	0.077819	0.000430	0.057409	0.298491	15.62 ± 0.22	38.68	12.69	0.317 ± 0.015
10C1417	1100 °C	0.003027	0.101337	0.000523	0.065244	0.340295	15.67 ± 0.45	27.56	14.42	0.277 ± 0.013
10C1420	1250 °C	0.001034	0.051542	0.000193	0.024444	0.126602	15.56 ± 0.48	29.29	5.40	0.204 ± 0.010
10C1421	1400 °C	0.001320	0.066758	0.000224	0.028022	0.145974	15.65 ± 0.77	27.23	6.19	0.180 ± 0.009

Information on Analysis	Results	40(r)/39(k) ± 2σ	Age ± 2σ (Ma)	MSW	39Ar(k) (% ,n)	K/Ca ± 2σ
MMA01 groundmass 1E10-10 groundmass	Weighted Plateau	5.2084 ± 0.0495 ± 0.95%	15.65 ± 0.16 ± 1.03%	0.08	73.93 7	0.258 ± 0.087
Mutton Mountain			External Error ± 0.30	2.45	Statistical T Ratio	
akj			Analytical Error ± 0.15	1.0000	Error Magnification	
Project = HLP Irradiation = OSU1E10	Total Fusion Age	5.5144 ± 0.0603 ± 1.09%	16.56 ± 0.19 ± 1.17%		11	0.401 ± 0.007
J = 0.0016723 ± 0.0000035			External Error ± 0.33			
FCT-3 = 28.030 ± 0.003 Ma			Analytical Error ± 0.18			

Incremental Heating		36Ar(a)	37Ar(ca)	38Ar(cl)	39Ar(k)	40Ar(r)	Age ± 2σ (Ma)	40Ar(r) (%)	39Ar(k) (%)	K/Ca ± 2σ
10C1348	400 °C	0.000220	0.000197	0.000000	0.000716	0.013444	57.10 ± 15.24	17.11	0.30	1.561 ± 1.142
10C1349	500 °C	0.000068	0.001085	0.000000	0.001708	0.025419	45.40 ± 6.28	55.93	0.71	0.677 ± 0.109
10C1350	600 °C	0.000105	0.007618	0.000011	0.009221	0.101527	33.70 ± 1.83	76.56	3.84	0.520 ± 0.029
10C1351	700 °C	0.000053	0.017843	0.000004	0.016263	0.160454	30.23 ± 0.81	91.08	6.76	0.392 ± 0.020
10C1353	800 °C	0.000063	0.053161	0.000021	0.039487	0.392163	30.43 ± 0.31	95.46	16.42	0.319 ± 0.015
10C1354	875 °C	0.000065	0.053039	0.000013	0.033437	0.329012	30.15 ± 0.47	94.48	13.91	0.271 ± 0.013
10C1355	950 °C	0.000101	0.067840	0.000018	0.037154	0.361124	29.78 ± 0.37	92.36	15.45	0.235 ± 0.011
10C1356	1000 °C	0.000094	0.053205	0.000017	0.027126	0.263103	29.72 ± 0.41	90.45	11.28	0.219 ± 0.011
10C1358	1050 °C	0.000090	0.037057	0.000000	0.018495	0.179612	29.76 ± 0.55	87.12	7.69	0.215 ± 0.010
10C1359	1100 °C	0.000082	0.035343	0.000010	0.016376	0.157902	29.55 ± 0.60	86.68	6.81	0.199 ± 0.009
10C1360	1175 °C	0.000126	0.032089	0.000024	0.014825	0.139866	28.92 ± 0.96	78.99	6.17	0.199 ± 0.010
10C1361	1250 °C	0.000176	0.027732	0.000000	0.012480	0.121462	29.83 ± 1.08	70.07	5.19	0.194 ± 0.009
10C1363	1325 °C	0.000134	0.018710	0.000003	0.008129	0.083155	31.33 ± 0.78	67.70	3.38	0.187 ± 0.009
10C1364	1400 °C	0.000204	0.011574	0.000003	0.004995	0.048727	29.89 ± 1.40	44.69	2.08	0.186 ± 0.009

Information on Analysis	Results	40(r)/39(k) ± 2σ	Age ± 2σ (Ma)	MSWD	39Ar(k) (% ,n)	K/Ca ± 2σ
MMD04 plag Tygh Valley 1E7-10 plag	Weighted Plateau	9.7146 ± 0.0663 ± 0.68%	29.77 ± 0.23 ± 0.77%	1.06	66.51 7	0.214 ± 0.019
Mutton Mountain			External Error ± 0.53	2.45	Statistical T Ratio	
akj			Analytical Error ± 0.20	1.0281	Error Magnification	
Project = HLP Irradiation = OSU1E10 J = 0.0017127 ± 0.0000033 FCT-3 = 28.030 ± 0.003 Ma	Total Fusion Age	9.8870 ± 0.0624 ± 0.63%	30.29 ± 0.22 ± 0.73%		14	0.248 ± 0.004
			External Error ± 0.53			
			Analytical Error ± 0.19			

Normal Isochron			39(k)/36(a) ± 2σ	40(a+r)/36(a) ± 2σ	r.i.
10C1394	500 °C	✓	1.2 ± 0.0	317.4 ± 3.2	0.8135
10C1395	600 °C	✓	4.9 ± 0.0	352.5 ± 2.4	0.8540
10C1397	700 °C	✓	7.1 ± 0.1	370.7 ± 4.7	0.8957
10C1398	800 °C	✓	10.2 ± 0.2	399.6 ± 8.2	0.9626
10C1399	900 °C	✓	12.8 ± 0.2	427.1 ± 5.4	0.9552
10C1401	1025 °C	✓	12.2 ± 0.2	424.4 ± 6.1	0.9392
10C1402	1150 °C		10.2 ± 0.1	408.2 ± 3.8	0.6919
10C1405	1275 °C		9.0 ± 0.2	400.2 ± 7.4	0.9112
10C1406	1400 °C		6.3 ± 0.3	376.2 ± 16.0	0.8822

Information on Analysis	Results	40(a)/36(a) ± 2σ	40(r)/39(k) ± 2σ	Age ± 2σ (Ma)	MSWD	40(a)/36(a) ± 2σ
MMR02 plag 1E6-10 plag Mutton Mountain akj Project = HLP Irradiation = OSU1E10 J = 0.0017218 ± 0.0000 FCT-3 = 28.030 ± 0.003 Ma	Isochron		305.7330 ± 2.6340 ± 0.86%	9.4582 ± 0.3550 ± 3.75%	29.14 ± 1.09 ± 3.74%	1.02
					External Error ± 1.18	
					Analytical Error ± 1.09	
	Statistics		Statistical F Ratio 2.37 Error Magnification 1.0122 n 6	Convergence Number of Iterations Calculated Line		0.0000000635 10 Weighted York-2

Incremental Heating		36Ar(a)	37Ar(ca)	38Ar(cl)	39Ar(k)	40Ar(r)	Age ± 2σ (Ma)	40Ar(r) (%)	39Ar(k) (%)	K/Ca ± 2σ
10C1376	500 °C	0.027480	0.014709	0.000291	0.043513	0.406191	28.40 ± 6.73	4.76	3.42	1.272 ± 0.071
10C1377	600 °C	0.003766	0.010446	0.000616	0.106968	1.000132	28.45 ± 0.36	47.33	8.41	4.403 ± 0.224
10C1378	650 °C	0.003363	0.009089	0.000895	0.142742	1.341901	28.60 ± 0.49	57.45	11.22	6.753 ± 0.335
10C1379	700 °C	0.002554	0.006912	0.000730	0.113885	1.063685	28.42 ± 0.40	58.49	8.95	7.085 ± 0.373
10C1381	750 °C	0.002897	0.007784	0.000822	0.134310	1.266237	28.68 ± 0.35	59.66	10.56	7.420 ± 0.371
10C1382	800 °C	0.003589	0.009157	0.000975	0.163017	1.515707	28.29 ± 0.70	58.83	12.82	7.655 ± 0.405
10C1383	850 °C	0.002810	0.007494	0.000894	0.132330	1.243025	28.58 ± 0.33	59.95	10.40	7.593 ± 0.380
10C1386	900 °C	0.001790	0.005246	0.000553	0.084024	0.788190	28.54 ± 0.25	59.84	6.61	6.888 ± 0.352
10C1387	975 °C	0.002067	0.005449	0.000606	0.095785	0.898872	28.55 ± 0.24	59.54	7.53	7.559 ± 0.396
10C1388	1050 °C	0.002045	0.005207	0.000620	0.092309	0.872242	28.75 ± 0.24	59.07	7.26	7.624 ± 0.392
10C1389	1150 °C	0.002090	0.004815	0.000577	0.086523	0.814507	28.64 ± 0.53	56.87	6.80	7.727 ± 0.418
10C1392	1275 °C	0.001403	0.002769	0.000409	0.052281	0.507503	29.53 ± 0.33	55.04	4.11	8.119 ± 0.631
10C1393	1400 °C	0.000877	0.001334	0.000178	0.024283	0.227920	28.56 ± 0.66	46.79	1.91	7.826 ± 1.032

Information on Analysis	Results	40(r)/39(k) ± 2σ	Age ± 2σ (Ma)	MSW	39Ar(k) (% ,n)	K/Ca ± 2σ			
MMR04 glass 1E8-10 glass	Weighted Plateau	9.3944 ± 0.0347 ± 0.37%	28.58 ± 0.15 ± 0.54%	0.43	93.98 11	2.838 ± 1.601			
Mutton Mountain							External Error ± 0.48	2.23	Statistical T Ratio
akj							Analytical Error ± 0.10	1.0000	Error Magnification
Project = HLP Irradiation = OSU1E10 J = 0.0017000 ± 0.0000034 FCT-3 = 28.030 ± 0.003 Ma	Total Fusion Age	9.3918 ± 0.0885 ± 0.94%	28.58 ± 0.29 ± 1.02%		13	6.050 ± 0.099			
			External Error ± 0.54						
			Analytical Error ± 0.27						

Incremental Heating		36Ar(a)	37Ar(ca)	38Ar(cl)	39Ar(k)	40Ar(r)	Age ± 2σ (Ma)	40Ar(r) (%)	39Ar(k) (%)	K/Ca ± 2σ
10C3361	500 °C	0.006606	0.006906	0.000971	0.050305	0.087767	4.83 ± 0.62	4.30	19.16	3.132 ± 0.106
10C3362	600 °C	0.003798	0.012833	0.001355	0.067226	0.109095	4.50 ± 0.36	8.86	25.60	2.252 ± 0.072
10C3363	700 °C	0.003083	0.020267	0.000926	0.050464	0.080012	4.39 ± 0.37	8.07	19.22	1.071 ± 0.034
10C3364	800 °C	0.003708	0.030012	0.000588	0.041546	0.069969	4.67 ± 0.45	6.00	15.82	0.595 ± 0.018
10C3366	900 °C	0.003141	0.026723	0.000211	0.019429	0.040452	5.77 ± 0.64	4.18	7.40	0.313 ± 0.010
10C3367	1050 °C	0.003825	0.038762	0.000205	0.017272	0.065463	10.49 ± 1.13	5.47	6.58	0.192 ± 0.006
10C3368	1200 °C	0.001413	0.032701	0.000113	0.009834	0.035245	9.92 ± 1.04	7.78	3.75	0.129 ± 0.004
10C3370	1400 °C	0.000838	0.019762	0.000092	0.006521	0.019219	8.16 ± 1.32	7.21	2.48	0.142 ± 0.004

Information on Analysis	Results	40(r)/39(k) ± 2σ	Age ± 2σ (Ma)	MSW	39Ar(k) (% , n)	K/Ca ± 2σ
TVF 16 glass Or jh	Weighted Plateau	1.6386 ± 0.0763 ± 4.65%	4.54 ± 0.21 ± 4.72%	0.63	79.80 4	0.831 ± 0.595
			External Error ± 0.23	3.18	Statistical T Ratio	
			Analytical Error ± 0.21	1.0000	Error Magnification	
Project = HLP Irradiation = OSU3B10	Total Fusion Age	1.9316 ± 0.0750 ± 3.88%	5.35 ± 0.21 ± 3.96%		8	0.601 ± 0.007
J = 0.0015380 ± 0.0000063			External Error ± 0.23			
FCT-3 = 28.030 ± 0.003 Ma			Analytical Error ± 0.21			

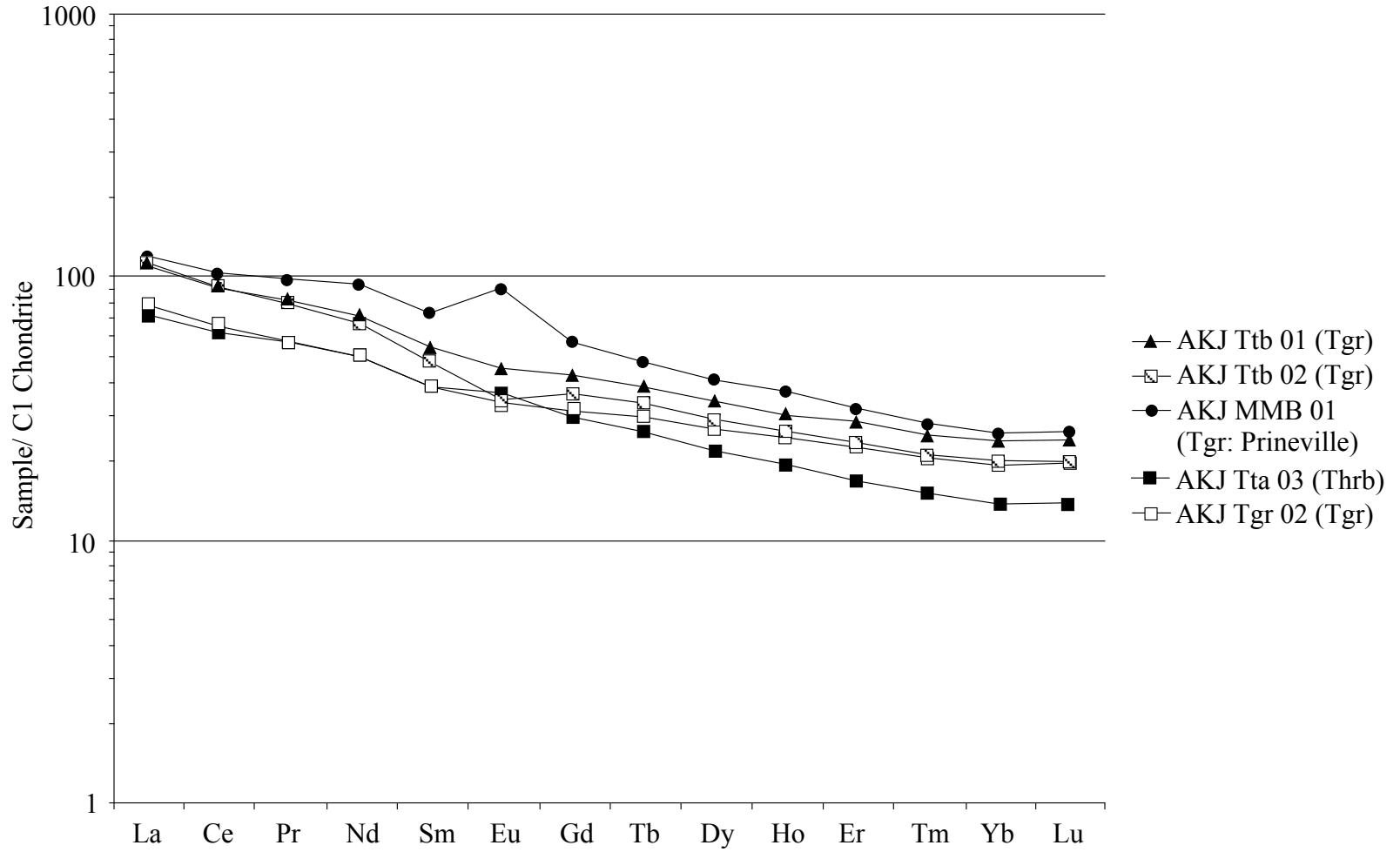
Incremental Heating		36Ar(a)	37Ar(ca)	38Ar(cl)	39Ar(k)	40Ar(r)	Age ± 2σ (Ma)	40Ar(r) (%)	39Ar(k) (%)	K/Ca ± 2σ
10C3324	400 °C	0.000498	0.003017	0.000047	0.000712	0.002044	7.68 ± 10.45	1.37	1.14	0.102 ± 0.014
10C3325	500 °C	0.000125	0.004068	0.000111	0.001695	0.004567	7.21 ± 4.78	10.97	2.72	0.179 ± 0.011
10C3326	600 °C	0.000108	0.016633	0.000312	0.004418	0.013849	8.38 ± 1.45	30.23	7.09	0.114 ± 0.005
10C3328	700 °C	0.000045	0.042653	0.000273	0.004657	0.014550	8.36 ± 1.50	52.09	7.48	0.047 ± 0.002
10C3329	800 °C	0.000081	0.110160	0.000240	0.007059	0.022171	8.40 ± 0.93	47.99	11.33	0.028 ± 0.001
10C3332	900 °C	0.000069	0.135755	0.000122	0.007031	0.022274	8.47 ± 0.72	52.12	11.29	0.022 ± 0.001
10C3333	1025 °C	0.000148	0.260484	0.000088	0.011926	0.037691	8.45 ± 0.46	46.34	19.15	0.020 ± 0.001
10C3334	1150 °C	0.000309	0.274490	0.000051	0.012213	0.038535	8.44 ± 0.58	29.68	19.61	0.019 ± 0.001
10C3336	1275 °C	0.000478	0.207810	0.000025	0.008697	0.027370	8.42 ± 0.55	16.24	13.96	0.018 ± 0.001
10C3337	1400 °C	0.000893	0.090326	0.000011	0.003868	0.006197	4.29 ± 1.63	2.29	6.21	0.018 ± 0.001

Information	Results	40(r)/39(k) ± 2σ	Age ± 2σ (Ma)	MSW	39Ar(k) (% , n)	K/Ca ± 2σ
TVF 17 glass Or jh	Weighted Plateau	3.1525 ± 0.0968 ± 3.07%	8.43 ± 0.27 ± 3.21%	0.04	93.79 9	0.021 ± 0.006
			External Error ± 0.30	2.31	Statistical T Ratio	
			Analytical Error ± 0.26	1.0000	Error Magnification	
Project = HLP Irradiation = OSU3B10 J = 0.0014861 ± 0.0000071 FCT-3 = 28.030 ± 0.003 Ma	Total Fusion Age	3.0389 ± 0.1238 ± 4.07%	8.13 ± 0.34 ± 4.18%		10	0.023 ± 0.000
			External Error ± 0.36			
			Analytical Error ± 0.33			

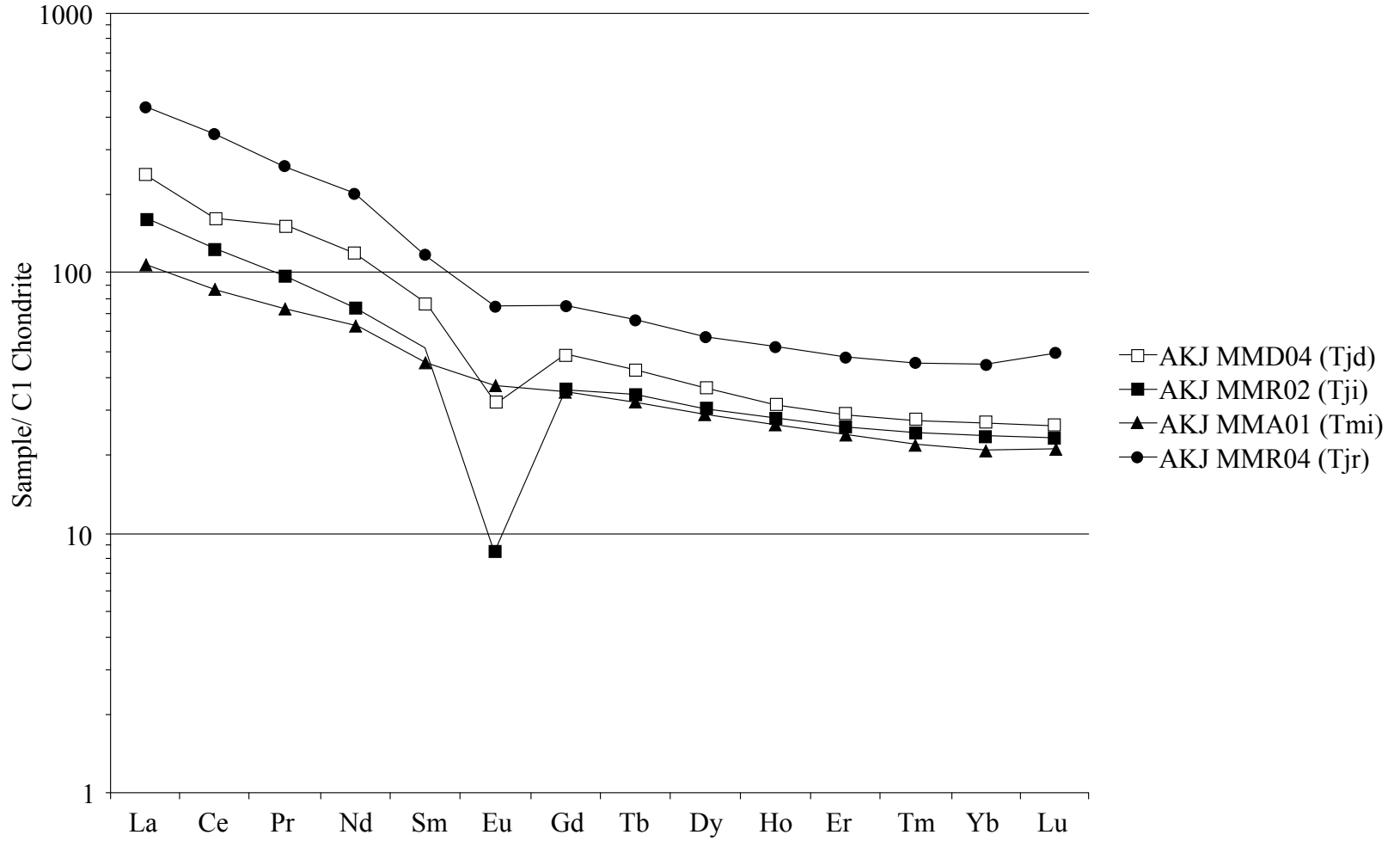
Incremental Heating		36Ar(a)	37Ar(ca)	38Ar(cl)	39Ar(k)	40Ar(r)	Age ± 2σ (Ma)	40Ar(r) (%)	39Ar(k) (%)	K/Ca ± 2σ
10C1366	500 °C	0.002327	0.017898	0.000016	0.001230	0.015139	37.07 ± 23.12	2.15	6.00	0.030 ± 0.001
10C1367	600 °C	0.004011	0.155489	0.000000	0.002710	0.011626	13.01 ± 17.68	0.97	13.22	0.007 ± 0.000
10C1368	700 °C	0.004644	0.258022	0.000000	0.003227	0.025504	23.88 ± 11.11	1.82	15.75	0.005 ± 0.000
10C1369	800 °C	0.008172	0.336345	0.000000	0.004053	0.028672	21.39 ± 16.31	1.17	19.78	0.005 ± 0.000
10C1371	900 °C	0.007055	0.238255	0.000000	0.002797	0.011648	12.63 ± 35.51	0.56	13.65	0.005 ± 0.000
10C1372	1025 °C	0.007232	0.241391	0.000000	0.002405	0.012813	16.14 ± 69.26	0.60	11.74	0.004 ± 0.000
10C1373	1150 °C	0.007369	0.187604	0.000014	0.001743	0.012323	21.38 ± 59.45	0.56	8.51	0.004 ± 0.000
10C1374	1400 °C	0.007808	0.270324	0.000017	0.002329	0.095600	120.76 ± 50.04	3.98	11.36	0.004 ± 0.000

Information on Analysis	Results	40(r)/39(k) ± 2σ	Age ± 2σ (Ma)	MSW	39Ar(k) (% , n)	K/Ca ± 2σ
TVF01 plag Tygh Valley 1E9-10 plag Tygh Valley akj	Weighted Plateau	7.3283 ± 2.4658 ± 33.65%	22.16 ± 7.41 ± 33.44%	0.53	88.64 7	0.005 ± 0.002
			External Error ± 7.42	2.45	Statistical T Ratio	
			Analytical Error ± 7.41	1.0000	Error Magnification	
Project = HLP Irradiation = OSU1E10 J = 0.0016865 ± 0.0000034 FCT-3 = 28.030 ± 0.003 Ma	Total Fusion Age	10.4092 ± 4.3546 ± 41.83%	31.40 ± 13.02 ± 41.47%		8	0.005 ± 0.000
			External Error ± 13.03			
			Analytical Error ± 13.02			

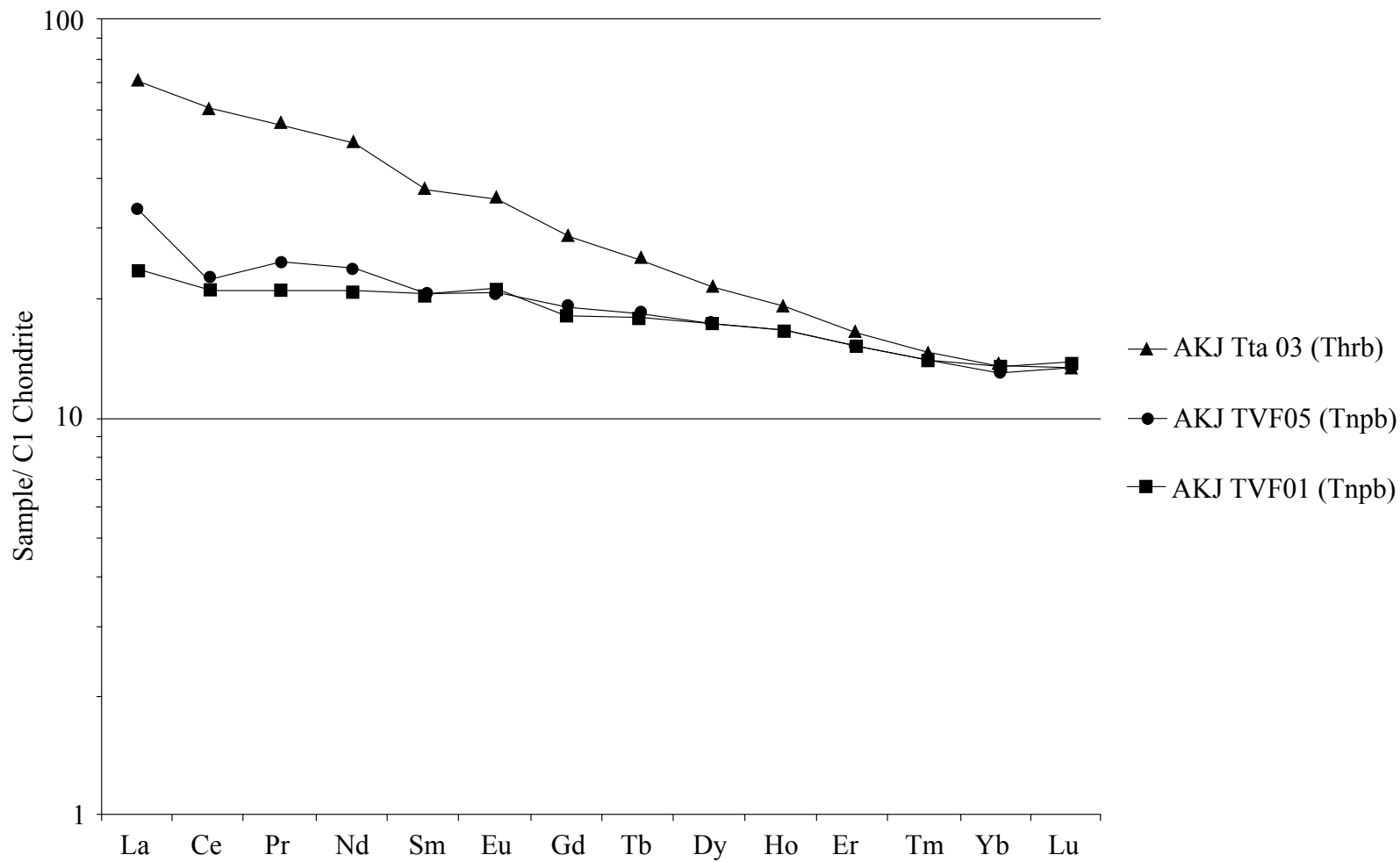
Appendix B: REE chart of all basalts



Appendix B: REE chart of Mutton Mountain units



Appendix B: REE Chart of Tygh Valley basalts



Appendix B: Geochemical Comparison of CRBG

	AKJ TVB-01 CRBG	AKJ TVB-02 CRBG	AKJ TGR-02 CRBG	AKJ MMB-01 CRBG (Prineville)	AKJ TVB-03 CRBG	Swanson CRBG Yakima	Donnelly- Nolan CRBG	Beeson Tygh Valley
Unnormalized Major Elements (Weight %):								
SiO2	51.30	54.91	52.70	53.38	51.28	50.90	50.30	53.30
TiO2	2.87	1.80	1.83	2.49	2.97	2.50	1.37	1.44
Al2O3	13.19	15.07	13.85	14.12	13.25	13.80	17.70	18.20
FeO*	13.79	9.05	11.47	9.80	13.86	10.80	9.65	8.63
MnO	0.22	0.19	0.22	0.22	0.21	0.14	0.15	0.13
MgO	4.32	4.48	4.92	3.39	4.34	4.70	7.02	4.88
CaO	8.25	7.15	8.91	6.33	8.23	7.60	10.10	8.77
Na2O	2.85	3.23	2.79	3.69	2.96	2.80	3.13	3.50
K2O	1.36	1.58	1.02	3.21	1.26	1.20	0.53	0.80
P2O5	0.58	0.27	0.29	1.47	0.57	0.66	0.36	0.30
Sum	98.72	97.73	98.00	98.09	98.94	95.10	100.31	99.95
Normalized Major Elements (Weight %):								
SiO2	51.97	56.18	53.77	54.42	51.83	53.52	50.14	53.33
TiO2	2.91	1.84	1.87	2.54	3.00	2.63	1.37	1.44
Al2O3	13.36	15.42	14.14	14.39	13.40	14.51	17.65	18.21
FeO*	13.97	9.26	11.70	9.99	14.01	11.36	9.62	8.63
MnO	0.22	0.20	0.22	0.22	0.21	0.15	0.15	0.13
MgO	4.38	4.59	5.03	3.45	4.39	4.94	7.00	4.88
CaO	8.36	7.32	9.10	6.45	8.32	7.99	10.07	8.77
Na2O	2.89	3.31	2.85	3.76	2.99	2.94	3.12	3.50
K2O	1.37	1.62	1.04	3.27	1.27	1.26	0.53	0.80
P2O5	0.58	0.28	0.29	1.50	0.57	0.69	0.36	0.30
Total	100.00	100.00	100.00	100.00	100.00	100.00	100.00	100.00
Unnormalized Trace Elements (ppm):								
Ni	19.20	48.40	17.80	17.80	21.30	20.00	89.00	N/A

Appendix B: Geochemical Comparison of CRBG

	AKJ TVB-01 CRBG	AKJ TVB-02 CRBG	AKJ TGR-02 CRBG	AKJ MMB-01 CRBG (Prineville)	AKJ TVB-03 CRBG	Swanson CRBG Yakima	Donnelly- Nolan CRBG	Beeson Tygh Valley
Cr	38.60	49.80	38.30	5.00	38.90	30.00	152.00	N/A
Sc	36.50	22.40	35.40	34.50	36.50	30.00	N/A	N/A
V	407.00	197.40	323.40	239.50	426.70	500.00	231.00	N/A
Ba	576.80	421.80	471.20	2255.60	560.30	500.00	207.00	N/A
Rb	33.40	66.80	22.60	44.50	34.30	N/A	7.00	N/A
Sr	317.60	294.60	323.90	299.30	314.30	300.00	429.00	N/A
Unnormalized Trace Elements (ppm), continued:								
Zr	200.30	249.90	153.30	137.30	191.90	150.00	118.00	N/A
Y	42.10	35.60	32.90	50.40	41.70	30.00	24.00	N/A
Nb	16.20	17.60	12.00	9.10	16.10	15.00	10.00	N/A
Ga	21.70	21.60	21.70	19.50	20.90	20.00	18.00	N/A
Cu	28.10	42.40	31.80	28.20	28.60	30.00	79.00	N/A
Zn	143.30	98.20	114.90	121.10	145.50	0.00	76.00	N/A
Pb	5.80	5.30	6.00	7.40	5.60	0.00	3.00	N/A
La	27.10	26.50	19.10	26.80	27.10	0.00	8.00	N/A
Ce	59.50	56.80	42.00	59.50	56.60	0.00	21.00	N/A
Th	3.80	4.50	2.10	2.90	3.30	0.00	2.00	N/A
Nd	33.60	28.20	23.90	42.20	31.20	N/A	12.00	N/A
U	1.30	3.20	0.40	2.70	1.30	N/A	2.00	N/A
sum tr.	2011.90	1691.00	1692.70	3403.30	2002.10			
in %	0.20	0.17	0.17	0.34	0.20			
sum m+tr	98.92	97.90	98.17	98.43	99.14			
M+Toxides	98.97	97.94	98.21	98.49	99.19			

**Major elements are normalized on a volatile-free basis, with total Fe expressed as FeO.
"R" denotes a duplicate bead made from the same rock powder.**

Appendix B: Geochemical Comparison of CRBG

Date	AKJ TVB-01 5-Apr-10	AKJ TVB-02 5-Apr-10	AKJ TGR-02 5-Apr-10	AKJ MMB-01 5-Apr-10	AKJ TVB-03 5-Apr-10	Swanson CRBG Yakima	Donnelly- Nolan CRBG	Beeson Tygh Valley
NiO	24.4	61.6	22.7	22.7	27.1	N/A	N/A	N/A
Cr2O3	56.4	72.8	56.0	7.3	56.9	N/A	N/A	N/A
Sc2O3	56.0	34.4	54.3	52.9	56.0	N/A	N/A	N/A
V2O3	598.7	290.4	475.8	352.3	627.7	N/A	N/A	N/A
BaO	644.0	470.9	526.1	2518.4	625.6	N/A	N/A	N/A
Rb2O	36.5	73.1	24.7	48.7	37.5	N/A	N/A	N/A
SrO	375.6	348.4	383.0	354.0	371.7	N/A	N/A	N/A
ZrO2	270.6	337.6	207.1	185.5	259.2	N/A	N/A	N/A
Y2O3	53.5	45.2	41.8	64.0	53.0	N/A	N/A	N/A
Nb2O5	23.2	25.2	17.2	13.0	23.0	N/A	N/A	N/A
Ga2O3	29.2	29.0	29.2	26.2	28.1	N/A	N/A	N/A
CuO	35.2	53.1	39.8	35.3	35.8	N/A	N/A	N/A

Major elements are normalized on a volatile-free basis, with total Fe expressed as FeO.

"R" denotes a duplicate bead made from the same rock powder.

ZnO	179.5	123.0	143.9	151.7	182.2	N/A	N/A	N/A
PbO	6.2	5.7	6.5	8.0	6.0	N/A	N/A	N/A
La2O3	31.8	31.1	22.4	31.4	31.8	N/A	N/A	N/A
CeO2	73.1	69.8	51.6	73.1	69.6	N/A	N/A	N/A
ThO2	4.2	5.0	2.3	3.2	3.6	N/A	N/A	N/A
Nd2O3	39.2	32.9	27.9	49.2	36.4	N/A	N/A	N/A
U2O3	1.4	3.5	0.4	3.0	1.4	N/A	N/A	N/A
Cs2O	0.0	0.0	0.0	0.0	0.0	N/A	N/A	N/A
As2O5	0.0	0.0	0.0	0.0	0.0	N/A	N/A	N/A
W2O3	0.0	0.0	0.0	0.0	0.0	N/A	N/A	N/A
sum tr.	2539	2113	2133	4000	2533			
in %	0.25	0.21	0.21	0.40	0.25			

Appendix B: Geochemical Comparison of Mutton Mountain rhyolites, Gray Butte John Day rhyolites

	AKJ MMR-04 Tjr	AKJ MMR-02 Tji	AKJ MMA-01 Tmi	AKJ MMD-04 Tjd	AKJ MMR-07 Tjd	Robinson_ JohnDayG	McClaghry Gray Butte rhyolite
Unnormalized Major Elements (Weight %):							
SiO2	73.05	76.06	55.51	68.93	64.66	76.90	N/A
TiO2	0.23	0.09	2.10	0.51	0.57	0.33	N/A
Al2O3	12.74	12.28	13.44	13.00	13.59	10.80	N/A
FeO*	2.02	1.12	12.11	4.63	8.10	0.12	N/A
MnO	0.02	0.02	0.20	0.09	0.14	0.01	N/A
MgO	0.05	0.03	3.42	0.33	0.11	0.10	N/A
CaO	0.76	0.63	6.96	2.15	3.35	0.60	N/A
Na2O	3.82	3.16	3.29	4.42	3.84	2.50	N/A
K2O	4.70	5.17	1.75	3.26	3.63	6.70	N/A
P2O5	0.04	0.02	0.36	0.09	0.12	0.02	N/A
Sum	97.43	98.59	99.13	97.40	98.11	98.08	N/A
Normalized Major Elements (Weight %):							
SiO2	74.97	77.15	55.99	70.77	65.90	78.41	76.83
TiO2	0.24	0.09	2.12	0.52	0.58	0.34	0.25
Al2O3	13.08	12.46	13.56	13.34	13.85	11.01	12.40
FeO*	2.08	1.14	12.22	4.75	8.26	0.12	1.31
MnO	0.02	0.02	0.20	0.09	0.15	0.01	0.01
MgO	0.05	0.03	3.45	0.34	0.11	0.10	0.10
CaO	0.78	0.64	7.02	2.21	3.41	0.61	0.37
Na2O	3.92	3.21	3.32	4.54	3.91	2.55	4.39
K2O	4.82	5.25	1.77	3.35	3.70	6.83	4.31
P2O5	0.04	0.02	0.36	0.10	0.12	0.02	0.03
Total	100.00	100.00	100.00	100.00	100.00	100.00	100.00

Appendix B: Geochemical Comparison of Mutton Mountain rhyolites, Gray Butte John Day rhyolites

	AKJ MMR-04 Tjr	AKJ MMR-02 Tji	AKJ MMA-01 Tmi	AKJ MMD-04 Tjd	AKJ MMR-07 Tjd	Robinson_ JohnDayG	Gray Butte rhyolite
Unnormalized Trace Elements (ppm), continued:							
Ni	3.80	3.70	14.50	4.70	4.70	0.00	15.00
Cr	3.10	3.90	4.60	5.00	2.20	1.50	8.00
Sc	6.40	2.30	33.20	12.60	20.80	N/A	5.00
V	4.20	5.10	361.70	21.20	3.90	7.00	3.00
Ba	918.10	289.70	712.80	856.70	2310.90	200.00	905.00
Rb	132.00	185.50	51.10	108.70	88.20	143.00	132.00
Sr	68.00	26.70	311.90	120.00	211.20	N/A	46.00
Zr	471.50	118.30	190.30	626.80	1177.30	1000.00	519.00
Y	41.30	42.20	37.30	68.00	68.30	50.00	64.00
Nb	29.30	20.40	13.70	31.80	36.10	30.00	68.00
Ga	24.50	22.90	21.90	24.80	29.00	20.00	27.00
Cu	4.10	5.80	24.20	7.70	17.40	7.00	3.00
Zn	95.50	46.30	126.70	120.20	195.00	0.00	135.00
Pb	16.00	21.00	9.90	13.80	12.90	10.00	16.00
La	53.20	38.30	23.20	54.40	99.90	70.00	N/A
Ce	94.20	68.50	52.00	110.80	198.80	70.00	N/A
Th	13.80	20.10	6.30	10.90	10.20	0.00	18.00
Nd	51.70	30.20	28.50	54.30	88.80	N/A	18.00
U	2.70	6.90	2.50	3.50	3.90	N/A	0.00
sum tr.	2033.40	957.80	2026.30	2255.90	4579.50	N/A	N/A
in %	0.20	0.10	0.20	0.23	0.46	N/A	N/A
sum m+tr	97.64	98.68	99.33	97.63	98.57	N/A	N/A
M+Toxides	97.68	98.70	99.38	97.68	98.66	N/A	N/A

Major elements are normalized on a volatile-free basis, with total Fe expressed as FeO.

"R" denotes a duplicate bead made from the same rock powder.

Appendix B: Geochemical Comparison of Mutton Mountain rhyolites, Gray Butte John Day rhyolites

	AKJ MMR-04 Tjr	AKJ MMR-02 Tji	AKJ MMA-01 Tmi	AKJ MMD-04 Tjd	AKJ MMR-07 Tjd	Robinson_ JohnDayG	McClaghry Gray Butte rhyolite
NiO	4.8	4.7	18.5	6.0	6.0	N/A	N/A
Cr2O3	4.5	5.7	6.7	7.3	3.2	N/A	N/A
Sc2O3	9.8	3.5	50.9	19.3	31.9	N/A	N/A
V2O3	6.2	7.5	532.1	31.2	5.7	N/A	N/A
BaO	1025.1	323.4	795.8	956.5	2580.1	N/A	N/A
Rb2O	144.4	202.9	55.9	118.9	96.5	N/A	N/A
SrO	80.4	31.6	368.9	141.9	249.8	N/A	N/A
ZrO2	636.9	159.8	257.1	846.7	1590.3	N/A	N/A
Y2O3	52.4	53.6	47.4	86.4	86.7	N/A	N/A
Nb2O5	41.9	29.2	19.6	45.5	51.6	N/A	N/A
Ga2O3	32.9	30.8	29.4	33.3	39.0	N/A	N/A
CuO	5.1	7.3	30.3	9.6	21.8	N/A	N/A
ZnO	119.6	58.0	158.7	150.5	244.2	N/A	N/A
PbO	17.2	22.6	10.7	14.9	13.9	N/A	N/A
La2O3	62.4	44.9	27.2	63.8	117.2	N/A	N/A
CeO2	115.8	84.2	63.9	136.2	244.4	N/A	N/A
ThO2	15.2	22.2	7.0	12.0	11.3	N/A	N/A
Nd2O3	60.3	35.2	33.2	63.3	103.6	N/A	N/A
U2O3	3.0	7.6	2.8	3.9	4.3	N/A	N/A
Cs2O	0.0	0.0	0.0	0.0	0.0	N/A	N/A
As2O5	0.0	0.0	0.0	0.0	0.0	N/A	N/A
W2O3	0.0	0.0	0.0	0.0	0.0	N/A	N/A
sum tr.	2438	1135	2516	2747	5501		
in %	0.24	0.11	0.25	0.27	0.55		

	AKJ TVF-05 Tnpb	AKJ TVF-01 Tnpb	AKJ TTA-03 Thrb	AKJ TVB-03 CRBG	Shears_Br dacite unknown
Unnormalized Major Elements (Weight %):					
SiO2	49.56	48.79	52.28	51.28	60.80
TiO2	1.28	1.40	2.07	2.97	0.85
Al2O3	17.23	17.20	16.67	13.25	16.90
FeO*	11.53	10.98	9.96	13.86	5.75
MnO	0.18	0.18	0.16	0.21	0.09
MgO	7.51	7.49	4.00	4.34	2.80
CaO	9.67	9.50	8.50	8.23	5.60
Na2O	3.07	2.82	3.81	2.96	4.01
K2O	0.25	0.30	0.89	1.26	1.41
P2O5	0.12	0.12	0.42	0.57	0.20
Sum	100.41	98.78	98.76	98.94	98.41
Normalized Major Elements (Weight %):					
SiO2	49.36	49.39	52.93	51.83	61.78
TiO2	1.27	1.42	2.09	3.00	0.86
Al2O3	17.16	17.41	16.88	13.40	17.17
FeO*	11.48	11.11	10.09	14.01	5.84
MnO	0.18	0.18	0.16	0.21	0.09
MgO	7.48	7.58	4.05	4.39	2.85
CaO	9.63	9.62	8.61	8.32	5.69
Na2O	3.06	2.86	3.85	2.99	4.07
K2O	0.25	0.30	0.90	1.27	1.43
P2O5	0.12	0.12	0.43	0.57	0.20
Total	100.00	100.00	100.00	100.00	100.00
Unnormalized Trace Elements (ppm):					
Ni	114.80	118.10	21.20	21.30	18.00
Cr	180.30	195.50	45.10	38.90	20.00
Sc	29.70	32.70	25.10	36.50	N/A
V	195.50	206.40	212.80	426.70	N/A
Ba	192.60	75.00	265.70	560.30	395.00
Rb	3.30	2.00	13.80	34.30	21.00
Sr	285.70	649.00	510.20	314.30	610.00
Zr	75.50	76.40	147.50	191.90	192.00
Y	24.50	23.30	26.80	41.70	23.00
Nb	5.60	5.50	13.80	16.10	N/A
Ga	18.30	18.00	20.70	20.90	N/A
Cu	46.90	55.50	41.50	28.60	28.00
Zn	87.90	86.40	100.00	145.50	60.00
Pb	1.80	0.60	2.50	5.60	
La	10.30	2.50	16.10	27.10	30.00
Ce	15.40	15.20	38.70	56.60	45.00
Th	0.00	0.00	1.70	3.30	N/A
Nd	10.30	10.40	23.10	31.20	N/A
U	1.50	0.30	0.60	1.30	N/A
sum tr. in %	1299.90 0.13	1572.80 0.16	1526.90 0.15	2002.10 0.20	

	AKJ TVF-05 Tnpb	AKJ TVF-01 Tnpb	AKJ TTA-03 Thrb	AKJ TVB-03 CRBG	Shears_Br dacite unknown
Unnormalized Trace Elements (ppm), continued:					
sum m+tr		100.54	98.94	98.91	99.14
M+Toxides		100.57	98.98	98.95	99.19
Major elements are normalized on a volatile-free basis, with total Fe expressed as FeO.					
"R" denotes a duplicate bead made from the same rock powder.					
NiO	146.1	150.3	27.0	27.1	N/A
Cr2O3	263.5	285.7	65.9	56.9	N/A
Sc2O3	45.6	50.2	38.5	56.0	N/A
V2O3	287.6	303.6	313.1	627.7	N/A
BaO	215.0	83.7	296.7	625.6	N/A
Rb2O	3.6	2.2	15.1	37.5	N/A
SrO	337.9	767.5	603.4	371.7	N/A
ZrO2	102.0	103.2	199.2	259.2	N/A
Y2O3	31.1	29.6	34.0	53.0	N/A
Nb2O5	8.0	7.9	19.7	23.0	N/A
Ga2O3	24.6	24.2	27.8	28.1	N/A
CuO	58.7	69.5	51.9	35.8	N/A
ZnO	110.1	108.2	125.2	182.2	N/A
PbO	1.9	0.6	2.7	6.0	N/A
La2O3	12.1	2.9	18.9	31.8	N/A
CeO2	18.9	18.7	47.6	69.6	N/A
ThO2	0.0	0.0	1.9	3.6	N/A
Nd2O3	12.0	12.1	26.9	36.4	N/A
U2O3	1.7	0.3	0.7	1.4	N/A
Cs2O	0.0	0.0	0.0	0.0	N/A
As2O5	0.0	0.0	0.0	0.0	N/A
W2O3	0.0	0.0	0.0	0.0	N/A
sum tr.	1680	2021	1916	2533	
in %	0.17	0.20	0.19	0.25	